University of Nottingham

UK | CHINA | MALAYSIA

Susceptibility of the human Nav1.7 voltage-gated sodium channel to pyrethroid insecticides

Seyedehmahsa Sharifnia

Thesis submitted to the University of Nottingham for the degree of Master of Research

April 2024

Abstract

Pyrethroid insecticides, generally regarded as low risk for human and mammalian toxicity, have paradoxically been associated with neurological symptoms among agricultural workers, including tingling, limb pain, unusual facial sensations, dizziness, and headaches. These symptoms are notably similar to those of primary erythromelalgia, a condition characterized by aberrant neuronal firing.

In this study, we utilized the TE671 cell line, which specifically expresses the $Na_V1.7$ sodium channel, to conduct whole-cell patch-clamp recordings. This method provided insight into the biophysical changes in the channel's activation, inactivation, and the emergence of tail currents upon repolarization, which are indicative of modifications induced by pyrethroids.

Our research unveiled that escalated concentrations of permethrin consistently caused a significant hyperpolarizing shift in the voltage of half-maximal activation (V_{50}), suggestive of enhanced channel sensitivity. Conversely, such a shift in the V_{50} was only observed with the highest tested concentration of deltamethrin. Flumethrin displayed a bidirectional influence on the V_{50}, with meaningful changes in both hyperpolarizing and depolarizing directions at specific concentrations. Notably, none of the pyrethroids markedly altered the fast inactivation phase.

Additionally, permethrin did not elicit prolonged tail currents, while deltamethrin and flumethrin did, in a concentration-dependent manner, with higher concentrations of flumethrin leading to greater channel modulation. This observation points to a potential gain-of-function effect in the $Na_V1.7$ channels, mirroring the pathophysiology of primary erythromelalgia.

The findings suggest that, at relevant concentrations, pyrethroids can induce functional changes in $Na_V1.7$ channel kinetics, which may underlie the sensory abnormalities reported in pyrethroid exposure. These alterations highlight a significant gain of function that could be instrumental in the symptomatology observed in exposed individuals, bringing attention to potential risks in the use of these widely applied insecticides.

Acknowledgement

I am profoundly grateful to the extraordinary individuals who have supported me throughout this educational journey.

To my supervisor, Dr Ian Mellor, your guidance, expertise, and unwavering support have been the cornerstone of my academic success. Your belief in my potential has been a source of inspiration, and your mentorship has been invaluable. Thank you for leading me through this challenging journey.

To my examiners, Dr Angus Brown and Dr Andrias O'Reilly, thank you for your time, effort, and insightful feedback. Your constructive critiques have significantly enhanced the quality of my work and have been crucial to the completion of this thesis.

To my husband, Mohammad, your unwavering strength, support, patience, and motivation have been my pillars throughout this entire journey. Your sacrifices, both big and small, have not gone unnoticed. From late nights and early mornings to managing countless responsibilities, you have been my steadfast partner, always there to lend a helping hand and offer words of encouragement. Your patience and understanding have given me the space to grow and succeed, and your motivation has fueled my perseverance and determination.

To my incredible mother, Maryam, your endless sacrifices, constant encouragement, and boundless love have been the foundation of my success. You have been my greatest champion, and your unwavering belief in my abilities has fuelled my ambition and determination. Your selflessness and dedication have inspired me more than words can express. I am forever grateful for everything you have done for me.

To my beloved grandparents, Mehri and Mohsen, your unparalleled generosity and steadfast love have profoundly impacted my life. Your support has opened doors to opportunities I could only dream of, and your wisdom has provided the strength to overcome countless challenges. Your presence in my life has been an immeasurable blessing.

To my wonderful younger brother, Mohammad, your youthful energy has been a great source of comfort and strength. Your encouragement has reminded me of the importance of perseverance, and I'm deeply grateful for your presence in my life.

Table of Contents

List of tables

List of Figure

1 INTRODUCTION

1.1 Overview of Pesticides

The term "pesticides" encompasses a variety of substances including insecticides, fungicides, herbicides, rodenticides, molluscicides, and nematicides, all of which are utilized for controlling different types of pests (1).

Pesticides play a crucial role in both public health, veterinary medicine and agriculture. They mitigate diseases by controlling harmful vectors like mosquitoes and pests in various environments, significantly reducing health risks. In agriculture, pesticides are vital for preserving crop yields, a necessity intensified by the growing global population. However, the application of pesticides must balance with environmental preservation, particularly concerning non-target species and biodiversity. Sustainable practices are essential, striving for a harmony where chemical pesticides remain a key tool, yet integrated with methods that safeguard ecological health (2).

Historically, pest control in agriculture evolved from manual and physical methods to chemical interventions, starting with arsenic and copper and advancing to synthetic compounds in the 1940s, such as DDT, followed by organophosphates and carbamates in the 1950s. These substances were effective but raised concerns due to their toxicity to non-target species. The development of synthetic pyrethroids in the 1970s marked a significant improvement, offering effective pest control with reduced mammalian toxicity (3).

Pesticides are categorized based on their target pests (e.g., fungicides, insecticides, herbicides, rodenticides), chemical composition (organic or inorganic), functional groups, modes of action, and toxicity levels. Inorganic pesticides include substances like copper sulfate and sulfur, while organic pesticides are diverse, encompassing various chemical structures like chlorohydrocarbons and organophosphates. Further classification is detailed by the specific chemical nature of organic pesticides, which include numerous subcategories such as carbamates and synthetic pyrethroids, each used extensively in agriculture (2).

1.1.1 Pyrethroids

Pyrethroid insecticides are widely used around the world for the control of indoor and agricultural pests, as well as vectors of diseases that affect both humans and animals. Their global application spans from protecting crops to combating disease-carrying insects such as mosquitoes.

Historically, the properties of the pyrethrum flower were harnessed as early as the 19th century, where tribes in the Caucasus and Persia utilized the blossoms to combat lice infestations. This natural form of insect control laid the groundwork for the development of synthetic analogues.

Derived from the naturally occurring insecticidal components in the flowers of *Tanacetum cinerariifolium*, pyrethroids are a class of synthetic compounds that have been optimized for increased efficacy and environmental stability. These enhancements are exemplified in the structural modifications of the six principal naturally occurring insecticidal esters known as pyrethrins. The molecular architecture of pyrethrins consists of a cyclopropane carboxylic acid and a cyclopentenolone alcohol component, which vary only at the terminal substituents. Within this group, three distinct alcohols - pyrethrolone, cinerolone, and jasmolone - are associated with the corresponding compounds: pyrethrins, cinerins, and jasmolins, respectively. Two critical acids, chrysanthemic acid and pyrethric acid, form the backbone of the Pyrethrins I and II series, respectively. These compounds are none-persistent in the environment and have low toxicity to mammals. They are known for their ability to rapidly knock down and kill insects, although they are not very stable and can be broken down by light and air (4). Figure 1.1 illustrates the chemical structures of pyrethrins and related compounds.

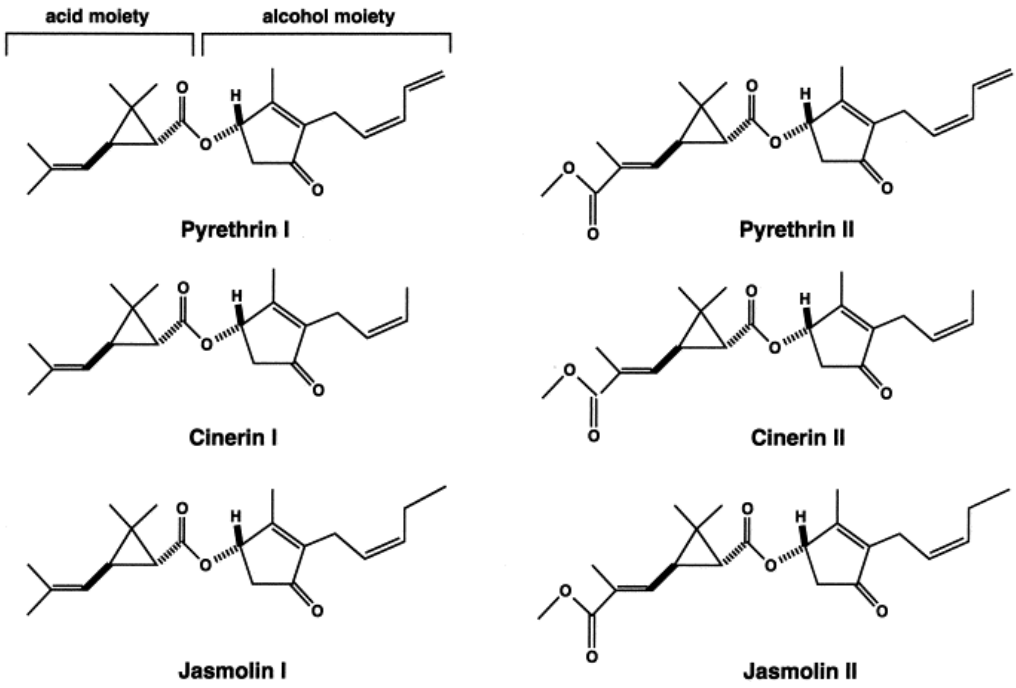

Figure 1.1: Structural Diagrams of the Six Insecticidal Esters Derived from Pyrethrum Extract: Pyrethrins I and II, Cinerins I and II, and Jasmolins I and II. (5)

Synthetic pyrethroids of the first and second generations were synthesized by modifying the alcohol portion of the chrysanthemic acid ester found in natural pyrethrins. These alterations were carefully designed to maintain the three-dimensional conformation and the physicochemical characteristics that are essential for pyrethrin's insecticidal and toxicological effectiveness. All pyrethroids share common structural elements, which include an acid moiety linked by an ester bond to an alcohol moiety. With two chiral centers in the acid part and potentially another in the alcohol part, pyrethroids often have several stereoisomeric forms. This molecular diversity leads to a total of eight possible stereoenantiomers for some pyrethroids. The efficacy of these compounds as insecticides, their acute neurotoxicity in mammals, and their impact on voltage-gated sodium channels are all influenced by the stereochemistry, implying that they interact with specific active sites in these systems. Commercially, there is a range of pyrethroid products with varying isomer compositions. For instance, the commercial product allethrin consists of a combination of all stereoisomers of allethrin. In contrast, d-allethrin comprises only the 1R isomers, bioallethrin is limited to the 1R-trans isomers, and S-bioallethrin is predominantly composed of the S enantiomer of the 1R-trans isomers (6).

1.1.2 Pyrethroid Exposure in Human

Pyrethroid exposure can occur through skin contact, inhalation, or ingestion, with various sources such as professional handling, contaminated water and food, and household products. Notably, the consumption of produce from treated areas has been associated with the detection of pyrethroid metabolites in human urine, highlighting a direct link between environmental application and human intake (7).

Individuals who handle pyrethroids in occupational settings often report paresthesia, characterized by sensations like numbness, itching, burning, or tingling, which are limited to areas of skin contact and not indicative of skin irritation. This induced paresthesia is generally transient and reversible, with symptoms lasting from several hours to occasionally up to two days. Despite the presence of these cutaneous sensations, clinical examinations of workers show no signs of acute pyrethroid intoxication, and physiological parameters for vital organs and systems remain within normal ranges. Furthermore, electrophysiological evaluations of peripheral nerve function have not demonstrated any abnormalities that can be attributed to occupational pyrethroid exposure. The onset of paresthesia is typically quick, occurring within half an hour of contact, and is confined to the skin exposure site, with no relation to the classical signs of skin irritation or systemic intoxication (5).

1.1.3 Classifying Pyrethroids Pesticides

Pyrethroid insecticides, widely used for their efficacy against a variety of pests, are categorized into two distinct types based on their chemical structure and resultant neurotoxic effects. Type I pyrethroids, such as permethrin, are characterized by the absence of an alpha-cyano group in their molecular structure. In contrast, Type II pyrethroids, exemplified by deltamethrin, incorporate an alpha-cyano group attached to the phenyl benzyl alcohol moiety. This structural distinction significantly influences their mode of action on the nervous system, specifically targeting voltage-gated sodium channels (8).

The neurotoxic symptoms associated with pyrethroid poisoning vary between the two types, primarily due to their differential effects on sodium channel behavior. Type I pyrethroids induce symptoms including tremors, incoordination, prostration, seizures, and in severe cases, fatality. These symptoms are attributed to the ability of Type I pyrethroids to provoke recurrent firing of action potentials in neurons in response to a single stimulus, a phenomenon known as the Type I poisoning syndrome (9).

On the other hand, Type II pyrethroids lead to more complex neurotoxic manifestations, such as hypersensitivity, choreoathetosis (involuntary movements), tremors, and paralysis, collectively referred to as the Type II choreoathetosis syndrome. This syndrome is characterized by symptoms including hyperactivity, a hunched back, salivation, tremors, and incoordination, which can progress to sinuous writhing movements. At the cellular level, Type II pyrethroids disrupt normal neuronal function by causing prolonged membrane depolarization and reducing cellular excitability, resulting in increased after-potentials and repetitive neuronal firing or excitation (9). Figure 1.2 displays the chemical structures of various Type I and Type II pyrethroids, emphasizing the structural differences between these two classes.

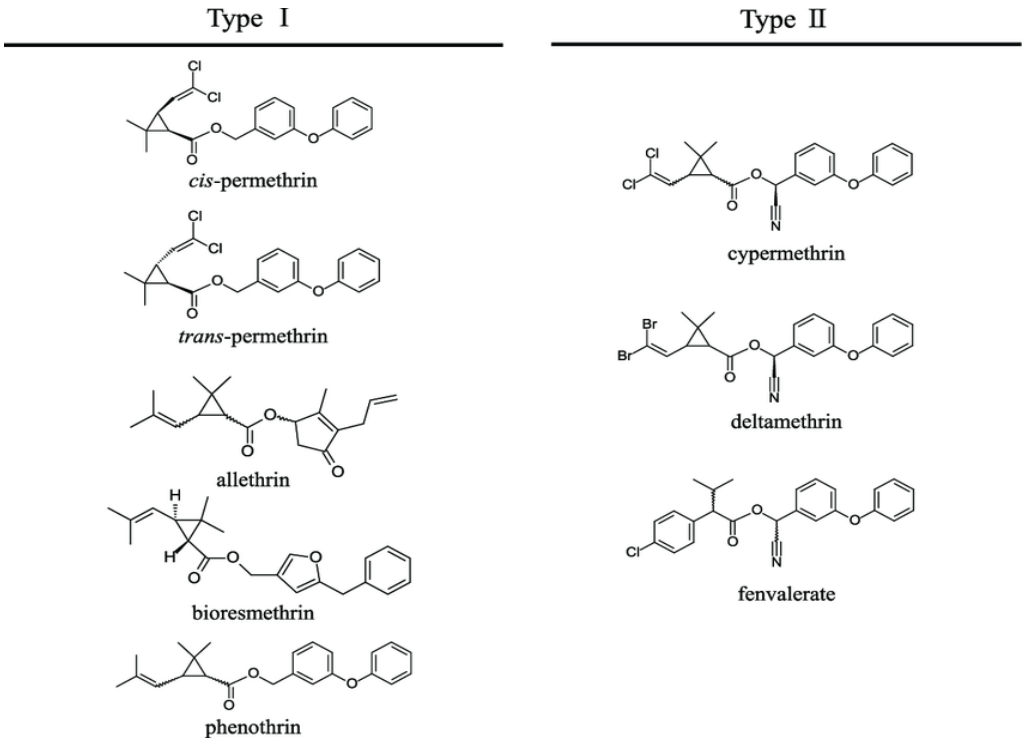

Figure 1.2: Molecular Structures of Type I and Type II Pyrethroids. The figure presents a clear distinction between Type I pyrethroids, which are characterized by their lack of a cyano group and include variants like cis-permethrin and bioresmethrin, and Type II pyrethroids that feature a cyano group contributing to their enhanced potency, such as cypermethrin and deltamethrin. Adapted from Fujino et al., 2019. (10)

1.1.4 Mode of Action of Pyrethroids

Pyrethroids disrupt the operation of Na^+ channel by causing a negative shift in the activation threshold (11), enabling them to open with minimal depolarization. They also decelerate the inactivation rate of Na^+, which is the process of inactivating these channels during depolarisation. Additionally, they delay the deactivation of these channels, prolonging their open state and enhancing neural excitability (9). Type II pyrethroids significantly prolong the deactivation phase of Na^+ compared to Type I pyrethroids. While Type I pyrethroids moderately extend the open state of these channels to facilitate repetitive neuronal firing, Type II pyrethroids induce an extensive delay in channel closure. This extended open state leads to sustained depolarization, effectively inhibiting the neuron's ability to generate subsequent action potentials—a phenomenon referred to as a depolarization-dependent block (6).

1.2 Voltage-gated Sodium Channels

Na^+ channels are heteromeric transmembrane proteins essential for the initiation and transmission of action potentials in excitable cells, including neurons, endocrine, cardiac myocytes, and skeletal muscle cells, by facilitating the entry of sodium ions (Na^+) into the cell upon activation (12, 13). These channels are not limited to excitable cells but are also found in nonexcitable cells like astrocytes, microglia, macrophages, and cancer cells, where they play roles in processes such as phagocytosis, cell motility, and metastatic activity, underscoring their involvement in a wide range of pathophysiological conditions (14, 15).

Na^+ channels first emerged evolutionarily in jellyfish, enabling efficient transmission of electrical signals in their dispersed neural network. While invertebrates primarily express Na^+ channels in the nervous system, chordates also feature them in striated muscle. Throughout evolution, the primary selective pressure for Na^+ channels has remained consistent: providing a solution for coordination and communication within large organisms, particularly when speed is crucial (16).
The exploration of Na^+ channels and their crucial role in neurophysiology unfolds a remarkable tale of innovation that traces back to the seminal contributions of Hodgkin and Huxley. Awarded the Nobel Prize for their groundbreaking discovery concerning action potentials in the squid's giant axon, their research set a cornerstone in the field of neuroscience. They devised the concept of ion-specific channels, an unprecedented breakthrough in grasping how neurons generate and transmit action potentials. In their 1952 study utilizing voltage clamp methods on the squid's giant axon, they illustrated that the onset of electrical signals in nerves is regulated by voltage-dependent sodium currents that facilitate the inward movement of Na^+ ions. These currents briefly activate and then deactivate within milliseconds, while the subsequent activation of voltage-gated potassium currents conducts K^+ ions outward, reinstating the membrane's initial electrical charge balance. This pioneering work unveiled the existence of voltage-gated sodium currents and laid the groundwork for subsequent investigations into this vital electrical signalling process (17-20).

During the 1980s, a significant breakthrough in electrophysiology was achieved with Erwin Neher and Bert Sakmann's introduction of the patch clamp technique. This

method facilitated the precise measurement of electrical currents through individual ion channels, providing details far beyond what previous techniques could offer. The patch clamp's ability to observe the functioning of single ion channels like those for sodium brought a revolutionary clarity to the understanding of ion channel dynamics (21).

While the function of the Na^+ channel was well-characterized through electrophysiological techniques by that era, its molecular structure and components remained less understood. The identification of the sodium channel protein relied heavily on employing neurotoxins, which bind to these channels with strong affinity, serving as crucial molecular markers (13). Beneski & Catterall pioneered this exploration by isolating two distinct size polypeptides from rat brain synaptosomes using α-scorpion toxin, revealing large α-subunits of about 260 kDa and smaller β-subunits of 30–40 kDa, setting a precedent for molecular characterization of the Na^+ channel (22).

Soon after, the purification of proteins from the electric eel's electroplax that bind tetrodotoxin showed a link between the activity of binding tetrodotoxin and a protein of approximately 270 kDa (23).

Progressing from this foundational work, Hartshorne & Catterall (1981) utilized saxitoxin to isolate and name α and β polypeptides in rat brain, correlating with Beneski & Catterall's findings and deepening the molecular insights into the channel's structure (24).

The narrative further evolved with the identification of an additional β subunit, termed β2, in later studies by Hartshorne & Catterall (1984) and Hartshorne et al. (1985), enhancing the conceptual model of the Na^+ channel as comprising a singular α-subunit paired with one or more β-subunits. Subsequent detailed purification studies illuminated these subunits' roles and their coordinated function, elucidating that an operative Na^+ channel includes these specific protein components, as described in Hartshorne & Catterall's comprehensive analyses during the mid-1980s (25, 26).

Together, these sequential advancements provided a clearer view of the Na^+ channel's molecular composition, marking significant progress from the initial electrophysiological insights into detailed structural delineation. This progression underscores a pivotal chapter in neuroscience research, bridging functional understanding with molecular specificity in the study of Na^+ channels.

1.2.1 Structural and Functional Complexity of Voltage-gated Sodium Channels (VGSCs)

The structure of Na^+ channel involves an α-subunit and one or more β-subunits. In 1984, Noda et al. accomplished a significant milestone in neurobiology by successfully cloning the gene for the alpha subunit of the Na^+ channel from the electric eel. This groundbreaking work not only revealed the primary structure of the sodium channel but also established a basis for understanding the molecular mechanisms underlying the generation and propagation of electrical signals in nerve and muscle tissues (27). The alpha subunit is the principal component responsible for sodium ion conduction across the cell membrane. It comprises four homologous domains (I-IV), each containing six transmembrane segments (S1-S6) and pore loop between S5 and S6. Within each domain, the S4 segment is enriched with positively charged arginine and lysine residues positioned at every third residue, crucial for the detection of voltage changes across the membrane (15). Movement of the S4 segment in response to voltage changes leads to conformational changes that open the channel. Upon depolarization, the S4 segments move outward, causing the channel to transition from a closed to an open state. Figure 1.3 shows the structure of a voltage-gated sodium channel, including the alpha subunit and associated beta subunits, highlighting key functional domains such as the voltage sensor, pore, and inactivation loop.

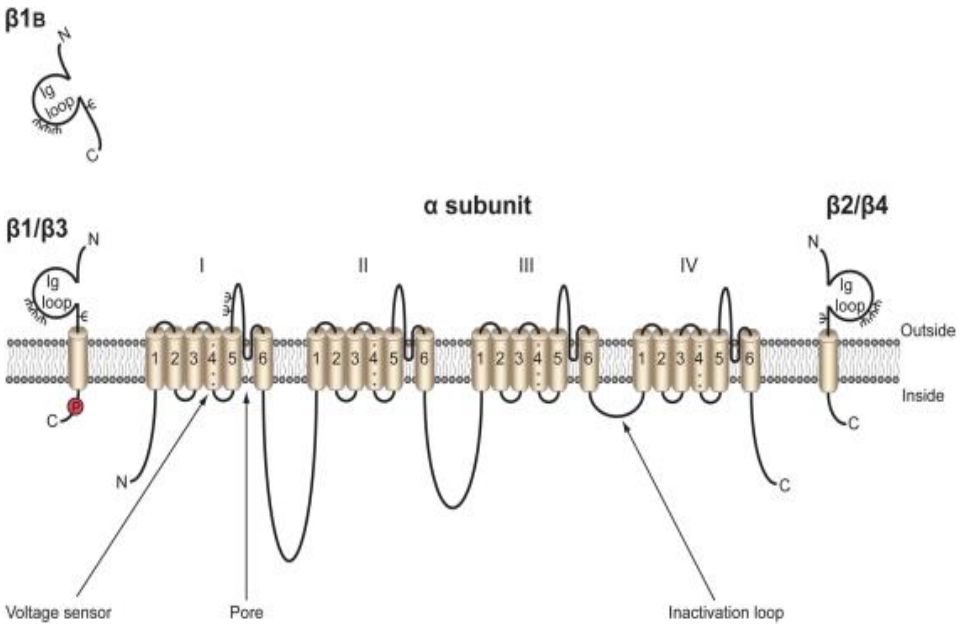

Figure 1.3 Structural Overview of Voltage-Gated Sodium Channel with Alpha Subunit and Associated Beta Subunits (28).

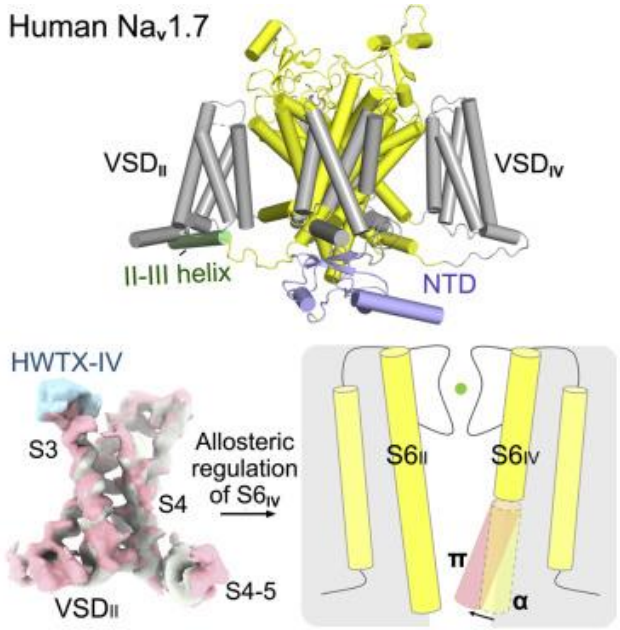

Figure 1.4 structure of the human $Na_v1.7$ channel. The 3D structure of the human $Na_v1.7$ channel showing the voltage-sensing domains in distinct colours.

The S5 and S6 segments across all domains collaboratively form the channel's pore, enabling the selective passage of Na^+ ions. The critical amino acid residues that contribute to selectivity are found in the P-loop region, which is situated in the loop

connecting S5 and S6, and lines the outer part of the pore. At the tips of the four P-loops where the outer pore is at its narrowest (29), the amino acids DEKA from DI-IV respectively form the selectivity filter. They interact with the permeating Na^+ ions, allowing the channel to differentiate Na^+ from other ions like K^+, based on the ion's charge density because of their different sizes. The internal half of the pore is lined by S5 and S6 helices and at the intracellular end, the S6 helices converge to form the activation gate. Linkage between the voltage-sensing S4 helices and this activation gate is through the S4-S5 linkers that form a cuff around the activation gate. At rest (S4 in its more intracellular location) the S4-S5 linkers push against the S6 helices, squeezing them together and occluding the inner end of the pore. Upon depolarisation of the cell membrane, S4 helices move to their more extracellular position, rotating the S4-S5 linkers so that they no longer squeeze the S6 helices together; the S6 helices then splay apart and sufficient space for ion permeation is created (29-31).

The recent elucidation of a 'phenylalanine gap' within the voltage sensor domain offers a nuanced perspective on the activation mechanism of sodium channels. This concept highlights a distinct hydrophobic region that may play a pivotal role in the stabilization and transfer of gating charges during the activation process. Specifically, the presence of a conserved phenylalanine residue demarcates a gap that could be integral to preventing unwanted proton transfer and establishing an energetic barrier conducive to discrete, switch-like transitions from closed to open states. Understanding this structural feature enriches our comprehension of the Na^+ channel voltage-sensing dynamics, emphasizing the sophistication and precision embedded within these crucial membrane proteins. Incorporating this advanced structural insight, we gain a more profound appreciation of the molecular choreography that underlies the activation of sodium channels, a process fundamental to the excitability of neurons and muscle cells (32-34).

A key feature of voltage-gated sodium (Na_v) channels is the rapid inactivation mechanism that occurs while the cell is still depolarized. This mechanism is crucial for the normal electrical activity of excitable cells, allowing the cell to return to its resting state after an action potential and thereby setting the stage for the next excitation.

Conventionally, the "hinged-lid" or "ball and chain" model described fast inactivation as a process where the loop between domains III and IV, containing the critical isoleucine-phenylalanine-methionine (IFM) motif, acts like a lid that blocks the channel pore swiftly after activation, thus preventing further ion flow. Mutations of the IFM motif, such as IFM to QQQ, were shown to eliminate fast inactivation (35, 36), while mutations like T to M destabilize it (37). This model suggested that upon cell membrane depolarization, this linker attaches to specific sites on the inner side of domains III and IV, blocking the inner side of the channel pore and inhibiting sodium ions from entering the channel (38). Pan et al. (2018) provided crucial insights into the mechanism of fast inactivation through their structural analysis of the $Na_v1.4$ channel. Their study demonstrated that the IFM motif does not directly occlude the pore. Instead, it inserts into a hydrophobic pocket formed by the S4-S5 linker and the S6 segment of domains III and IV, supporting an allosteric blocking mechanism rather than a direct occlusion of the pore. This interaction stabilizes the inactivated state of the channel, preventing further sodium ion flow (39). Shen et al. (2019) extended these findings with high-resolution structures of the $Na_v1.7$ channel. They showed that the IFM motif in the III-IV linker inserts between the S4-5 linker and the S6 segment of domains III and IV. This supports the idea of an allosteric interaction rather than direct pore blockage, emphasizing the conformational flexibility of the S4-S5 linkers, which play a critical role in the fast inactivation process (40). Wu et al. (2023) provided further structural details on $Na_v1.7$ pharmacology, illustrating how the IFM motif and the surrounding regions interact with various pharmacological agents. Their work highlighted the significance of the surrounding residues and structural elements in modulating fast inactivation and the binding of pharmacological agents, offering potential therapeutic insights (41).

The research by Capes et al. (2013) meticulously investigates the role of the voltage sensor in domain IV (DIV) in the inactivation process of sodium channels, unveiling its indispensable and rate-limiting roles. The study delineates that the activation movement of this particular domain is not merely a participant but a requisite trigger for channel inactivation, asserting that DIV's behaviour alone can sufficiently induce the channel to transition into its inactivated state. This discovery highlights the

distinct role of DIV, positioning it as an essential pivot in the inactivation mechanism, in stark contrast to other domains whose contributions, though important, do not independently govern the inactivation process (42).

Furthermore, Capes et al. (2013) establish that the kinetics of DIV are intrinsically tied to the overall inactivation timeline, marking this domain's movement as the rate-limiting step in both the onset and recovery phases of fast inactivation. This characterization imbues DIV with a pivotal function, suggesting that its timely and precise movements are essential for the proper temporal orchestration of channel inactivation and reactivation, ensuring that sodium channels efficiently transition between conductive and non-conductive states in response to cellular signals. Notably, the study offers a nuanced perspective on closed-state inactivation, proposing that DIV's activation prior to the channel's opening facilitates inactivation from a closed state. This mechanism enriches our comprehension of sodium channel operation, particularly under varying physiological conditions, and highlights the sophisticated interplay of structural and electrical dynamics within the channel (42).

In contrast to fast inactivation, slow inactivation is a more prolonged process and might stem from ongoing structural adjustments within the channel when there is extended depolarization. These structural changes implicate several components of the channel, including its pore region, the S4 voltage-sensing segments in domains III and IV, and the IFM motif. During these extended periods of depolarization, the S4 segments in domains III and IV are posited to shift gradually, prompting a reconfiguration of the pore region that effectively blocks the sodium ion conduction pathway. This additional shift in the S4 voltage sensors diminishes the interaction strength between the IFM motif and its corresponding binding site (43). Slow inactivation contributes to the overall refractory period, influencing the frequency and pattern of action potential firing. This type of inactivation provides a second, longer-term layer of regulation over sodium channel activity, ensuring the fine-tuning of neuronal excitability and the prevention of excessive firing (38).

The β-subunits (β1-β4) play crucial roles in modulating various aspects of the α-subunit's functionality within voltage-gated sodium channels. They are instrumental in fine-tuning the α-subunit's expression levels, gating properties, and

pharmacological responsiveness, ensuring the channel operates optimally under diverse physiological conditions. These subunits also significantly contribute to the proper localization and stabilization of the sodium channels in the cell membrane, facilitating their appropriate distribution and anchorage. In terms of channel dynamics, the β-subunits affect the activation and inactivation processes, modifying the speed and voltage sensitivity with which the channels respond to electrical signals. Beyond their direct impact on channel function, they engage in cell adhesion processes and interact with extracellular matrix components, thereby influencing cellular connectivity and signal transduction. Through these multifaceted roles, the β-subunits are integral to the comprehensive regulation and integration of sodium channel activities within the cellular and extracellular environment (44).

1.2.2 Diversity and Functionality of Sodium Channels

In mammals, at least nine distinct isoforms of voltage-gated sodium channels ($Na_V1.1$ to $Na_v1.9$) have been identified, each exhibiting unique tissue distribution and functional properties. Moreover, because of the differences in amino acid sequence between isoforms, they also have subtle differences in channel properties (45, 46). Specifically, the isoforms $Na_v1.1$, $Na_v1.2$, $Na_v1.3$, and $Na_v1.6$ are predominantly expressed in the central nervous system (CNS), playing essential roles in neuronal excitability and signal transduction (47, 48). Conversely, $Na_v1.7$, $Na_v1.8$, and $Na_v1.9$ are primarily localized within the peripheral nervous system (PNS), where they are integral to pain sensation and peripheral nerve signalling (49, 50). The $Na_v1.4$ and $Na_v1.5$ subtypes are chiefly localised to the skeletal and cardiac muscles, respectively, where they are pivotal in muscle contraction and cardiac electrical activity (51, 52).

These isoforms are recognized for their distinct electrophysiological and pharmacological features, underlining their critical contribution to the specialized functions of sodium channels in various mammalian tissues and cell types (44, 53).

1.3 $Na_v1.7$ Isoform

The initial identification and cloning of the $Na_V1.7$ isoform were conducted using human neuroendocrine cells, denoted as hNE-Na. This discovery highlighted $Na_V1.7$'s

evolutionary connection, bridging the gap between the Na^+ channel previously characterized in skeletal muscle and those found in the brain, suggesting a conserved structural and functional lineage across diverse tissues (54). The $Na_V1.7$ channel in humans, which is encoded by the SCN9A gene, consists of a complex structure made up of 1977 amino acids. The intracellular loop between domains DI and DII, along with the carboxyl (COOH) terminus, exhibits specific sequences and structural motifs that are not found in other sodium channels. These distinctions are believed to confer unique regulatory and interaction properties to $Na_V1.7$, affecting how it responds to cellular signals and its pharmacological profile (54). While $Na_v1.7$ was originally thought to be mainly found in the peripheral nervous system (PNS), the Trombley and Westbrook (1991) research has revealed its presence in various regions of the central nervous system (CNS). Olfactory sensory neurons are among these CNS locations where $Na_v1.7$ has been identified (55).

Herzog et al. (2003) investigated $Na_v1.6$ and $Na_v1.7$ channels in mouse DRG neurons, revealing that $Na_v1.7$ exhibits notably slower closed-state inactivation than Nav 1.6, influencing their responses during extended or gradual depolarizations. Due to this slower inactivation, $Na_v1.7$ channels can remain active for extended periods during slow depolarizations, allowing them to react to incremental membrane potential changes, which $Na_v1.6$ may not detect. Consequently, $Na_v1.7$ can sustain larger subthreshold currents during these slow depolarizations compared to $Na_v1.6$, potentially heightening neuronal responsiveness to subtle, slow-changing stimuli. This function of $Na_v1.7$, particularly its ability to boost generator potentials and assist in the onset of neural impulses, underscores its critical role in sensory neurons, where it may influence processes like sensory detection and pain transmission (56).

Cummins et al. (1998) analysed the behaviours of $Na_v1.7$ and $Na_v1.4$ channels within HEK-293 cells, discovering that their activation responses to depolarization were remarkably similar. This was evidenced by comparable activation kinetics, with midpoint values at −25.8 mV for $Na_v1.7$ and −27.0 mV for $Na_v1.4$. However, distinct differences were noted in their inactivation kinetics: $Na_v1.7$ displayed a slower inactivation process with a time constant of 0.77 ms at 0 mV, in contrast to $Na_v1.4$'s faster 0.51 ms time constant and demonstrated a deeper voltage requirement for

reaching steady-state inactivation. Such differences imply that $Na_v1.7$ can sustain activation for longer durations and necessitates greater hyperpolarization to switch to its inactivated state, potentially amplifying its capacity to enhance and extend the duration of neuronal signalling (57).

The SCN9A gene, responsible for encoding the $Na_V1.7$ sodium channel, plays a crucial role in pain perception regulation, as evidenced by multiple studies. Variations in this gene lead to a range of genetic disorders related to pain. The dysfunctions in $Na_V1.7$, stemming from these mutations, can be categorized into two types: gain-of-function and loss-of-function. Gain-of-function mutations are associated with conditions like primary erythromelalgia (IEM) and paroxysmal extreme pain disorder (PEPD), recently, variants exhibiting gain-of-function have also been linked to more frequently occurring acquired pain conditions, including small fiber neuropathy and painful diabetic neuropathy. whereas loss-of-function mutations contribute to a rare condition known as congenital insensitivity to pain (CIP) (58-60).

IEM, inherited as an autosomal dominant trait, leads to heightened activity of voltage-gated sodium channels. It represents the first instance of a human pain disorder identified as being directly linked to a mutation in an ion channel (61).

IEM is characterized by symptoms including recurring burning pain, heightened warmth, and redness in the extremities. Electrophysiological studies consistently reveal that this condition involves a notable shift in the half-maximal voltage-dependence of activation towards more negative potentials. This shift makes the sodium channels overly responsive to even minor depolarizations, thereby lowering the threshold required for their activation. Such electrophysiological changes in sodium channel behaviour underscore the pathophysiological basis of IEM, contributing to its distinct symptomatology (62-64). Furthermore, the rate of deactivation is reduced, and ramp currents are increased (65).

PEPD, a disorder inherited in an autosomal dominant manner, is caused by missense mutations in the SCN9A gene. It manifests as episodic pain in the rectal, ocular, and/or submaxillary regions. Unlike the alterations in half maximal activation voltage seen in IEM, mutations associated with PEPD lead to a destabilization of fast inactivation,

characterized by a depolarizing shift in the voltage required for half maximal fast inactivation towards higher, more positive values (66, 67). This results in a greater number of channels being in a closed, resting (and thus activatable) state rather than in a closed, inactivated state, thereby increasing the neuron's excitability. Likely due to destabilized inactivation, PEPD mutant channels further amplify resurgent sodium currents (62).

Mutations that inactivate both alleles of SCN9A, the gene coding for the voltage-gated sodium channel $Na_V1.7$, lead to the remarkable clinical presentation of CIP (68).

1.4 The TE671 Cell Line: A Model for Studying $Na_v1.7$

The TE671 cell line, initially characterized as originating from cerebellar medulloblastoma but later reassigned as rhabdomyosarcoma (69), prominently expresses the SCN9A gene related to the $Na_V1.7$ sodium channel. This discovery, confirmed by qRT-PCR and western blot analyses, indicates a non-canonical, highly dominant expression of $Na_V1.7$ (70). Electrophysiological studies revealed that these cells generate voltage-sensitive sodium currents, which are crucial for studying the pharmacology of $Na_V1.7$, a target for developing analgesic drugs. The cell line's maintenance is cost-effective and straightforward, making it an excellent model for pain research (70).

1.5 Aims and Objectives

The primary objective of this research is to explore the effects of pyrethroid insecticides on human VGSCs, focusing specifically on the $Na_V1.7$ subtype found in sensory neurons. This investigation aims to deepen our understanding of the mechanisms by which these prevalent insecticides influence human VGSCs, especially $Na_V1.7$, and to illuminate the potential neurological implications and health risks stemming from exposure to pyrethroids.

The study will use whole cell patch clamp of TE671 cell to assess the impact of a broad spectrum of pyrethroids, encompassing both Type I and Type II classifications, on the functionality of the $Na_V1.7$ channels within human cells. Key aspects of this evaluation

include observing variations in channel activation and inactivation dynamics, as well as detecting the emergence of tail currents as a consequence of pyrethroid interaction.

2 MATERIALS AND METHODS

2.1 Reagents and Chemicals

Dulbecco's modified Eagle's medium (DMEM), fetal bovine serum (FBS), L-glutamine, Penicillin-Streptomycin, and trypsin/EDTA, catalogue number T4049, were acquired from Sigma Aldrich, UK. Trypsin/EDTA Solution were acquired from BioReagent for cell detachment, a trypsin/EDTA solution was utilized, comprising 0.25% (w/v) trypsin and 0.02% (w/v) EDTA, diluted in Hank's Balanced Salt Solution (HBSS) with phenol red for pH indication. This formulation contained 2.5 g of porcine trypsin and 0.2 g of EDTA tetrasodium salt per litre. The solution was sterile-filtered, ensuring it was free of any potential microbial contamination, and designated as a BioReagent, confirming its suitability for use in cell culture applications.

Permethrin, identified as 3-phenoxybenzyl (RS)-cis-trans-3-(2,2-dichlorovinyl)-2,2dimethyl-cyclopropanecarboxylate, was sourced from Sigma. To prepare a stock solution, 3.913 mg of permethrin, with a molecular weight of 391.3, was dissolved in 10 mL of dimethyl sulphoxide (DMSO, also acquired from Sigma) to achieve a concentration of 10^{-3} M.

Deltamethrin, known chemically as (S)-α-cyano-3-phenoxybenzyl(1R,3R)-3-(2,2-dibromovinyl)-2,2-dimethylcyclopropanecarboxylate, was procured from Sigma. A stock solution of 10^{-3} M concentration was prepared by dissolving 5.052 mg of deltamethrin (having a molecular weight of 505.2) into 10 mL of dimethyl sulphoxide (DMSO).

Flumethrin is chemically described as Cyano(4-fluoro-3-phenoxyphenyl) methyl 3-[2-chloro-2-(4-chlorophenyl)ethenyl]-2,2-dimethylcyclopropanecarboxylate was acquired from Sigma. A 10 mL stock solution with a concentration of 10^{-3} M was prepared by dissolving 5.104 mg of flumethrin (with a molecular weight of 510.38) in 10 mL of dimethyl sulphoxide (DMSO).

2.2 Cell Culture

TE671 cells were procured and revived from their cryogenic state in liquid nitrogen. These cells were cultured in (DMEM) containing 4.5 g/L glucose, enriched with 10% Serum (FBS), 10 IU/mL penicillin, 20 µg/mL streptomycin, and 2 mM glutamine for nourishment. During cell passaging, TE671 cells were exposed to 2 mL of trypsin/EDTA for 3 minutes at 37°C to facilitate detachment. Subsequently, the cells were gently separated and resuspended in 10 mL of whole culture medium. This suspension was then transferred into a 30 mL universal tube and subjected to centrifugation at 1000 rpm for 7 minutes. The resultant cell pellet was homogeneously combined with 10 mL of fresh culture medium. A portion of 0.5 mL from this mixture was allocated to a new 25 cm^2 culture flask containing 4.5 mL of culture medium and incubated at 37°C under a 5% CO_2 atmosphere. Two drops of cell suspension in DMEM were introduced into several 35 mm petri dishes, each containing 2 mL of the medium for patch-clamping.

2.3 Electrophysiology study

2.3.1 Bath Solution

For whole cell patch clamping experiments the media in the petri dishes were replaced with bath solution. This bathing solution had the following millimolar (mM) composition: 135 NaCl, 5.4 KCl, 1 $CaCl_2$, 1 $MgCl_2$, 5 HEPES, and 10 D-glucose. The pH was adjusted to 7.4 using NaOH.

2.3.2 Pipette Solution

A standard internal solution filled the pipettes. This solution comprised (in mM): 140 CsCl, 10 NaCl, 1 $MgCl_2$, 11 EGTA, and 5 HEPES. The pH was set to 7.2 by adjusting with CsOH.

2.3.3 Patch-pipettes

Patch pipettes were fabricated to achieve resistances ranging from 9 to 13 MΩ. The pipettes were crafted using a Sutter-P97 micropipette puller, designed to heat and

stretch borosilicate glass capillaries into the precise shape and resistance required for the measurements.

2.3.4 Whole Cell Patch Clamping

For visualization, we employed a Nikon Eclipse TE200 inverted microscope (from Nikon Corporation, Japan), which was situated on an anti-vibration platform within a Faraday cage. This setup included several wires grounding all metallic parts to reduce electrical interference. The microscope rested on an isolated, nitrogen-infused air table which maintained a nitrogen pressure of 50-60 psi to diminish vibrational impacts on the microscope's stage. The recording of currents was performed with a HEKA EPC 10 patch clamp amplifier (from HEKA Elektronik Dr. Schulze GmbH, Germany), utilizing the HEKA Pulse software for acquisition (Digitimer Ltd., Welwyn Garden City, Hertfordshire, UK). The amplifier's headstage was attached to a micromanipulator from Burleigh Products Group Inc, PCS-5000 series, NY, USA. We used a silver wire coated with silver chloride (AgCl) as the reference electrode, which was connected to the amplifier's ground input on one end and submerged into the bath solution on the other. Data transfer between the amplifier and the computer was facilitated by an LIH 1600 interface (HEKA Elektronik Dr. Schulze GmbH, Germany), which also served to convert data from analogue to digital formats and back. Currents across the membrane were acquired at a sampling rate of 20 kHz and subjected to a low-pass filter with a 5 kHz cutoff. Data collection commenced no sooner than three minutes following the establishment of the whole-cell configuration, ensuring sufficient time for the internal pipette solution to reach equilibrium with the cell's cytoplasm.

For the application of pyrethroids to TE671 cells, firstly the culture media was replaced by bathing solution and then 20 microliters of a pyrethroid stock solution in DMSO was added to the petri dish to achieve specific working concentrations. This mixture was allowed to incubate for 15 minutes, permitting sufficient time for the pyrethroids to mix uniformly in the bath solution. Following this incubation period, the cells were subjected to the whole-cell patch clamp procedure.

2.4 Voltage Protocol

2.4.1 Voltage Protocol 1

This protocol, illustrated in Figure 2.1, was designed to explore the activation voltage-dependency of voltage-gated Na^+ channels under the influence of pyrethroids, as well as in their absence. Starting with the TE671 cells at a holding potential of -80 mV, the protocol increased the voltage to various test potentials through a depolarization step of 25 ms. The range for test potentials was set from -80 mV up to +40 mV, adjusting in increments of 5 mV. In the current study, we used a starting voltage of -80 mV for our voltage protocols, as shown in Figure 2.1. This starting potential was chosen based on the typical resting membrane potential of neurons, which is physiologically relevant.

This protocol will reveal the peak sodium current (I_{peak}) at each test potential, allowing for the construction of a current-voltage (I-V) relationship. By transforming the I-V plot into a conductance-voltage (G-V) plot, key parameters such as the maximum conductance (G_{max}), reversal potential (V_{rev}), half-activation voltage ($V_{50.act}$), and slope factor (k) can be determined. These parameters are essential for understanding the voltage-dependent activation properties of the $Na_v1.7$ channels.

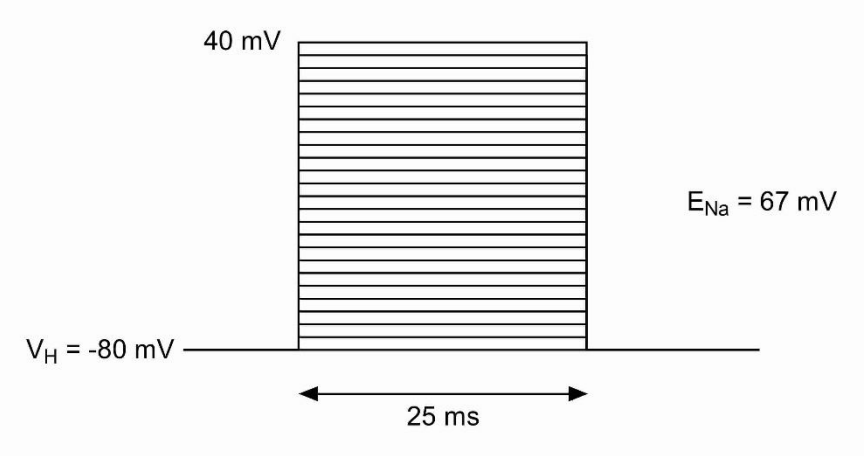

In Figure 2.1, Voltage Protocol 1 is depicted, showcasing the initial holding potential set at -80 mV, succeeded by a depolarization step lasting 25 ms, with test potentials incrementing from -80 mV to +40 mV by 5 mV steps.

2.4.2 Voltage protocol 2

The method depicted in Figure 2.2 facilitated the investigation of the voltage-dependence of steady state fast inactivation in voltage-gated Na^+ channels with and without the presence of pyrethroids. The TE671 cells were set to a holding potential of -80 mV prior to the delivery of 200 ms inactivation pre-pulses varying from -130 mV to +20 mV in 10 mV steps, which were directly succeeded by a 10 ms test pulse to -10 mV before reverting to the holding potential -80 mV.

This protocol will measure the peak sodium current (I_{peak}) at -10 mV following each inactivating pre-pulse. By normalising the current to maximum peak current (I_{max}), a normalised current versus inactivation voltage relationship can be plotted. This allows for the determination of the half-inactivation voltage ($V_{50.inact}$) and the slope factor (k), providing insight into the voltage dependence of fast inactivation of the $Na_v1.7$ channels.

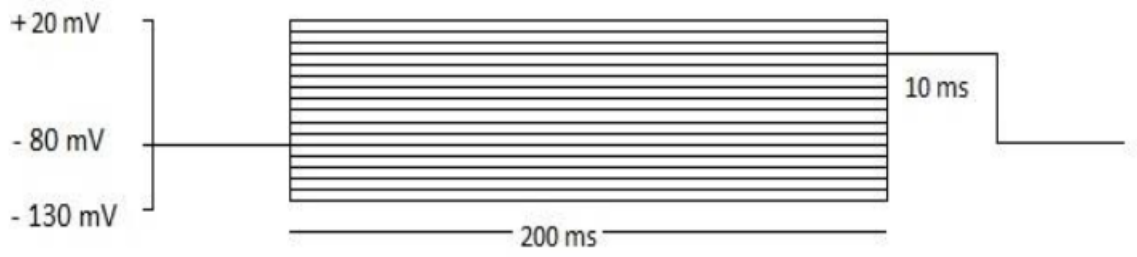

Fig 2.2 Voltage Protocol 2 is depicted as initiating with a holding potential of -80 mV. This is followed by a series of 200 ms conditioning pulses ranging from -130 mV up to +20 mV, increasing in 10 mV steps. At the conclusion of the protocol, a 10 ms test pulse to -10 mV is applied.

2.4.3 Voltage protocol 3

Tail currents are observed when there is a repolarising change in membrane potential, typically following a depolarizing pulse. These currents occur due to the delayed inactivation and deactivation of ion channels by pyrethroids that had been previously opened during the depolarization. This leads to a transient flow of ions (tail current) as the channels transition from the open to the closed state is delayed.

The methodology outlined in Figure 2.3 was utilized to investigate a notable effect of pyrethroid treatment on voltage-gated Na^+ channels, specifically the tail currents. Tail currents represent a significant impact of pyrethroids on these channels. Initially, the cells were set to a holding potential of -80 mV, which is close to the resting membrane potential of TE671 cells. The equilibrium potential for sodium (E_{Na}) in this setup is approximately +67 mV. The protocol involved 100 depolarizing pulses to 0 mV, each lasting 5 ms with a frequency of 66 Hz, allowing the Na^+ channels to transition between open and closed states rapidly. Following this, a 12-second repolarization pulse to -110 mV was applied.

Tail currents were measured during this repolarization phase, as the membrane potential transitioned from the depolarized state at 0 mV to the hyperpolarized state at -110 mV. This significant difference from E_{Na} (-110 mV vs. +67 mV) creates a strong driving force for Na^+ ions to enter the cell, resulting in observable tail currents. These currents are larger than those during the conditioning pulse due to the increased driving force for Na^+ ions when moving from a depolarized to a hyperpolarized state.

This protocol is designed to enhance the detection of tail currents, which are indicative of pyrethroid-induced modifications in the channels. The tail current observed during the repolarization phase (to -110 mV) provides information on how pyrethroids affect the inactivation and deactivation kinetics of $Na_V1.7$ channels. Parameters such as the amplitude and duration of the tail currents can be used to quantify the extent of channel modification.

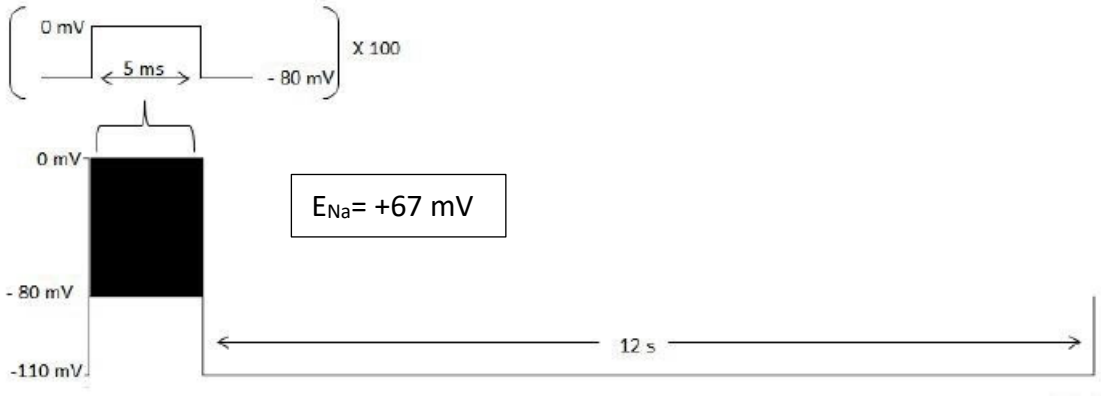

Fig 2.3 Voltage Protocol 3 illustrates an initial clamped potential set at -80 mV, succeeded by a sequence of 100 conditioning pulses of 5 ms each to 0 mV. To explore the inactivation

or deactivation of voltage-gated Na^+ channels, a 12-second repolarization pulse to -110 mV was included at the end of the protocol.

2.5 Data Analysis

Data analysis and visualization were conducted using GraphPad Prism 9 (GraphPad Software, La Jolla, CA, U.S.A.). The sample size, denoted as n, corresponds to the number of distinct experimental cells utilized.

In accordance with Voltage Protocol 1 (illustrated in Figure 2.1), the maximum current observed at each voltage step was charted against the testing voltage to establish a current-voltage (I-V) profile. To facilitate a comprehensive comparison, the data underwent normalization to mitigate variance in current magnitudes across different cells. This preparatory step was followed by an application of a revised Boltzmann equation (Equation 1), culminating in a detailed I-V curve depiction.

Equation 1:

$$I_{\text{peak}} = G_{\max}\left(\frac{V_T - V_{\text{rev}}}{1 + \exp\left(\frac{V_T - V_{50.\text{act}}}{k}\right)}\right)$$

This equation describes the peak sodium current (I_{peak}) elicited by a step depolarization to a test potential (V_T). It includes the maximum sodium conductance (G_{max}), which represents the highest conductance the channels can achieve; the reversal potential (V_{rev}), where there is no net sodium ion flow; the half-activation voltage ($V_{50.act}$), the potential at which half of the channels are open; and the slope factor (k), indicating the voltage sensitivity of channel activation. This equation is a product of a linear instantaneous current-voltage (I-V) relationship and the activation curve described by the Boltzmann equation. The numerator represents the driving force for sodium ions, and the denominator models the voltage-dependence of sodium channel activation. The peak current thus represents the flow of sodium ions through open channels at a specific voltage.

Recordings from Voltage Protocol 1 also enabled the fitting of a normalised conductance-voltage (G-V) relationship. Maximum conductance (G_{max}) and reversal potential (V_{rev}) values for baseline-corrected peak current data from each cell were calculated using Equation 1. The normalised conductance (G / G_{max}) for each value of test potential (V_T) was calculated from baseline-corrected data for each cell using the equation 2.

Equation 2:

$$\frac{G}{G_{\max}} = \frac{I_{\text{peak}}}{G_{\max}(V_T - V_{\text{rev}})}$$

This equation normalizes the conductance of the sodium channels, providing a quantity (G / G_{max}) that simplifies comparison across different conditions and cells. Here, I_{peak} is the peak sodium current evoked by the voltage step depolarization test potential (V_T), G is the conductance at V_T, G_{max} is the maximum sodium ion conductance, and V_{rev} is the reversal potential. By dividing the peak current by the driving force (V_T - V_{rev}) and normalising by the maximum conductance (G_{max}), this equation isolates the effects of voltage on channel conductance, independent of the

absolute current magnitude. The mean and SEM of these data provide the mean normalised conductance (G / G_{max}) for each test potential (V_T). These values are then fitted using Boltzmann sigmoidal equation (Equation 3) to create a conductance-voltage (G-V) relationship curve, allowing for the determination of the half-activation ($V_{50.act}$) based on conductance.

Equation 3:

$$\frac{G}{G_{\max}} = G_{\min} + \frac{G_{\max} - G_{\min}}{1 + \exp\left(\frac{V_{50.\text{act}} - V_T}{k}\right)}$$

This equation describes the normalised conductance (G / G_{max}) as a function of the depolarising step test potential (V_T). The normalised conductance transition from a minimum value (G_{min}) to a maximum value (G_{max}), with $V_{50.act}$ representing the half-activation potential and *k* as the slope factor indicating voltage sensitivity.

Following Voltage Protocol 2, the peak current (I_{peak}) recorded at each inactivating pre-pulse ($V_{T.inact}$) was normalised by dividing it by the maximum peak current (I_{max}) elicited from a series of -10 mV test depolarization pulses (V_T). This normalisation accounted for differences in current amplitude across different cells, yielding the normalised current (I_{peak} / I_{max}) used to assess the voltage-dependece of fast inactivation mechanisms.

The normalised current (I_{peak} / I_{max}) was plotted against the inactivating pre-pulse potential ($V_{T.inact}$) and fitted with a Boltzmann equation (Equation 4). This fitting allowed for the determination of the half-inactivation voltage ($V_{50.inact}$), the voltage at which half of the Na^+ channels in a cell are inactivated.

Equation 4:

$$\frac{I_{\text{peak}}}{I_{\max}} = I_{\min} + \frac{I_{\max} - I_{\min}}{1 + \exp\left(\frac{V_{50.\text{inact}} - V_{T.\text{inact}}}{k}\right)}$$

This equation models the normalized peak sodium current (I_{peak} / I_{max}) as a function of the inactivating pre-pulse potential ($V_{T.inact}$). Here, I_{peak} is the peak sodium current amplitude given by a single $V_{T.inact}$ pre-pulse, and I_{max} is the maximal peak current elicited for a series of V_T test pulses. The normalised current varies from a minimum

value (I_{min}) to a maximum value (I_{max}), with $V_{50.inact}$ representing half-inactivation potential, the voltage at which 50% of the channels are inactivated, and k as the slope factor indicating voltage sensitivity in mV.

Following Voltage Protocol 2, the peak current (I_{peak}) measured at each inactivating pre-pulse ($V_{T.inact}$) was normalised by dividing it by the maximum peak current (I_{max}) obtained from a series of -10 mV test pulses (V_T). This normalised accounted for variations in current amplitude across different cells, yielding the normalised current (I_{peak} / I_{max}) used to evaluate the voltage-dependence of fast inactivation mechanisms.

The normalised current (I_{peak} / I_{max}) was then plotted against $V_{T.inact}$ and fitted with the Boltzmann equation (Equation 4). This fitting allowed for determination of $V_{50.inact}$, the voltage at which half of the Na^+ channels in a cell are inactivated.

Research aiming to assess the response of voltage-gated sodium (Na^+) channels to pyrethroids involved determining the proportion of altered channels (M) through measurement of their tail currents using the following Equation 5 (Tatebayashi and Narahashi, 1994).

Equation 5:

$$M\% = \left(\frac{I_{tail}}{(V_{hold} - V_{rev})G_{max}}\right) \times 100$$

In this section, I_{tail} denotes the maximum intensity of the tail current observed at the repolarizing step V_{tail} (-110 mV), while V_{rev} represents the reversal potential for the sodium (Na^+) current, and G_{max} is the peak sodium conductance in the cell. Both V_{rev} and G_{max} were derived by applying a modified Boltzmann function (Equation 1) to the current-voltage (I-V) relationship data collected from each cell under investigation. The peak tail current's amplitude was assessed in relation to a 'baseline' zero level, established in the absence of any pyrethroid compounds. Recent research, such as that conducted by Burton et al. in 2011, has introduced Equation 6 for further evaluating the tail current. This approach calculates the integral modification (MI), offering an analysis that incorporates the tail current's duration, a factor not considered by Equation 5 (71).

Equation 6:

$$MI(\%) = \left(\frac{I_{\text{tail.integral}}}{(V_{\text{tail}} - V_{\text{rev}}) \cdot G_{\text{max}}}\right) \times 100$$

In this analysis, $I_{tail.integral}$ is defined as the product of the tail current's negative peak amplitude and its time constant, representing the total area under the tail current curve. MI, expressed as a percentage, was plotted against varying concentrations of pyrethroid.

3 Results

3.1 Sodium Current

TE671 cell line is an easy to maintain and cost-effective model for the study of $Na_V1.7$, a major target for the development of analgesic drugs and more generally for the study of pain (70).

Figure 3.1 shows a normalised peak current-voltage (I-V) relationship of the peak currents. From the graph, the currents were activated at voltages more positive than -70 mV and the maximum currents recorded were obtained at test potentials between 0 mV to 20 mV. The peak I-V relationship was fitted with a modified Boltzmann equation giving the reversal potential (Vrev) of the currents as +210.7 mV. Following the I-V plot of the current, the voltage-dependence of activation was examined by transforming the I-V plot into conductance versus voltage (G-V). The G-V plot was fited by a Boltzmann sigmoidal giving a $V_{50.act}$ of -22.40 mV with a slope factor (k) of 10.01 mV.

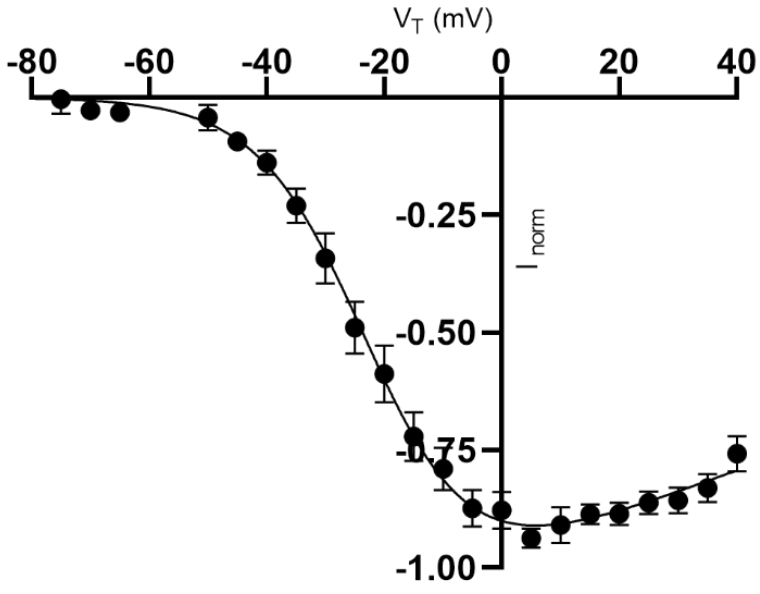

Figure 3.1 Voltage-current (I-V) characteristics of TE671 cell voltage-gated sodium channels documented through Voltage Protocol 1 and modeled with Equation 1. The reversal potential (V_{rev}) is +210.7 mV.

3.2 Activation

To analyse the voltage-dependence of activation, we transformed the current-voltage (*I-V*) plot into a conductance-voltage (*G-V*) plot. Conductance at each voltage point is calculated using Ohms' law, where conductance is the ratio of the current (*I*) to the voltage (*V*):

$$G = \frac{I}{V - V_{rev}}$$

Here, *I* is the measured current at a given Voltage *V*, and V_{rev} is the reversal potential, which is the voltage at which there is no net flow of sodium ions. The conductance values are then normalized to the maximum conductance (G_{max}) observed across all voltages to facilitate comparison across different conditions. The normalized conductance (G / G_{max}) is calculated as:

$$\frac{G}{G_{max}} = \frac{I}{(V - V_{rev})G_{max}}$$

The normalized conductance values (G / G_{max}) are plotted against the corresponding voltage (*V*) values to create the G-V curve. This plot illustrates how conductance changes with voltage and allows for the determination of key parameters such as the half-maximal activation voltage ($V_{50.act}$) and the slope factor (*k*). The G-V curve is fitted with using a Boltzmann function to accurately describe the voltage-dependence of channel activation:

$$\frac{\mathrm{G}}{\mathrm{G_{max}}} = \frac{1}{1 + \exp\left(\frac{\mathrm{V_{50.act}} - \mathrm{V}}{\mathrm{k}}\right)}$$

Based on the current-voltage information, the $V_{50.act}$ value for activation and the corresponding slope factor (k) for $hNa_V1.7$ in TE671 cells were determined using Equations 1, 2, and 3. The calculated $V_{50.act}$ and slope factor (k) values were -22.40 mV and 9.43 mV, respectively. Figure 3.2 illustrates the conductance-voltage relationship.

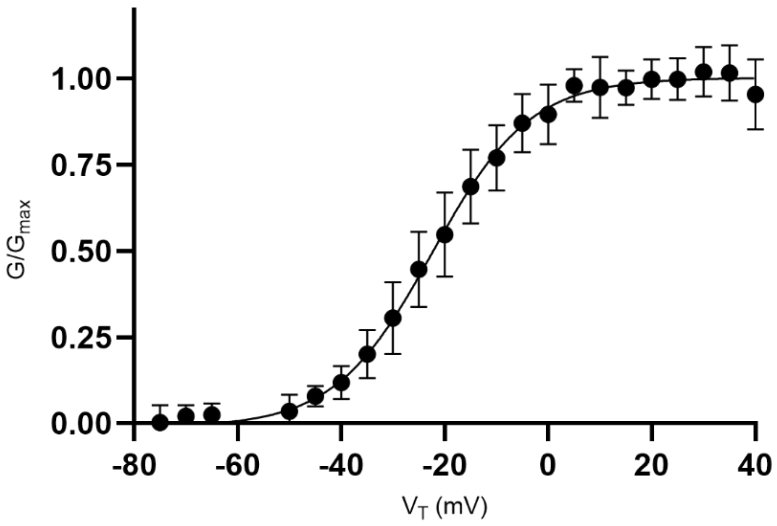

Figure 3.2 depicts the conductance-voltage curves for hNa$_V$1.7 in TE671 cells, obtained using Voltage Protocol 1 and analyzed with Equation 3. The $V_{50\text{-}act}$ is -22.40 mV, and the slope factor (k) is 9.43 mV.

3.3 Fast Inactivation

The voltage-dependence of fast inactivation was investigated by using Voltage Protocol 2. The normalised current-voltage (pre-pulse) relationship is shown in Figure 3.3. The value for $V_{50.inact}$ of the $hNa_V1.7$ for TE671 cells, calculated using Equation 4, was -88.83 mV.

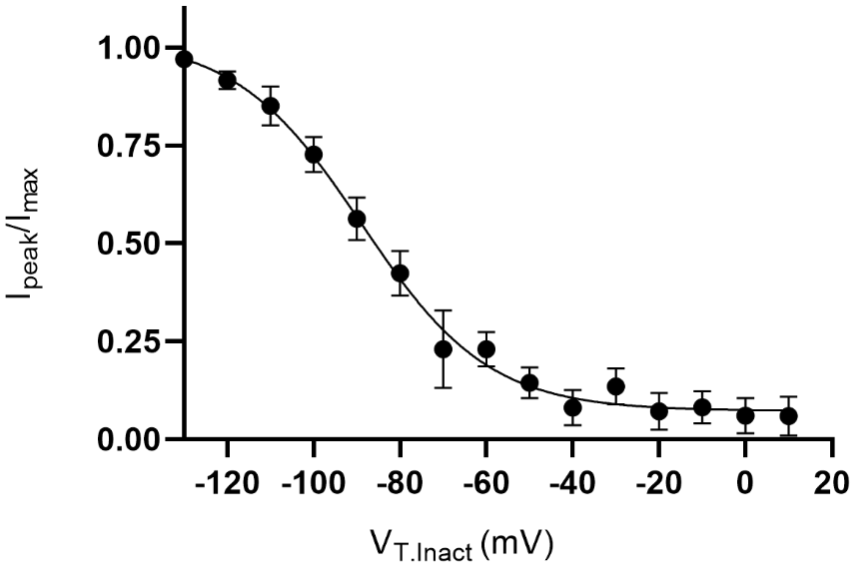

Figure 3.3 This graph depicts the normalized current-voltage relationship from Voltage Protocol 2, showcasing the fast inactivation process. The half-inactivation voltage ($V_{50\cdot inact}$) for $hNa_V1.7$ within TE671 cells is determined to be -88.83 mV with a slope factor (k) of 14.66 mV, as calculated using Equation 4.

3.4 Responsiveness to Pyrethroid Compounds

3.4.1 Influence of Pyrethroid Compounds on Sodium Ion Current

To assess the impact of pyrethroids on Na^+ currents facilitated by human $Na_V1.7$, different pyrethroids including Flumethrin, Deltamethrin, and Permethrin were administered externally at varying concentrations (ranging from 100 µM to 10 nanomolar) to TE671 cells. The Na^+ currents were then observed using Voltage Protocol 1.

The current-voltage (I-V) relationship was assessed by stepping the membrane potential from -80 mV to +40 mV, and the resulting peak sodium currents were plotted. The control group, without any pyrethroid treatment, established the

baseline I-V curve, against which the effects of the pyrethroids were measured. Permethrin at concentrations of 10 µM and 1 µM resulted in a negative shift in the current-voltage relationship. In contrast, a concentration of 100 nM of permethrin led to a depolarizing shift. Flumethrin at a concentration of 1 µM induced a depolarizing shift in the current-voltage relationship, whereas at 100 nM, flumethrin caused a hyperpolarizing shift. The highest tested concentration of deltamethrin (10 µM) produced a significant hyperpolarizing shift in the current-voltage relationship.

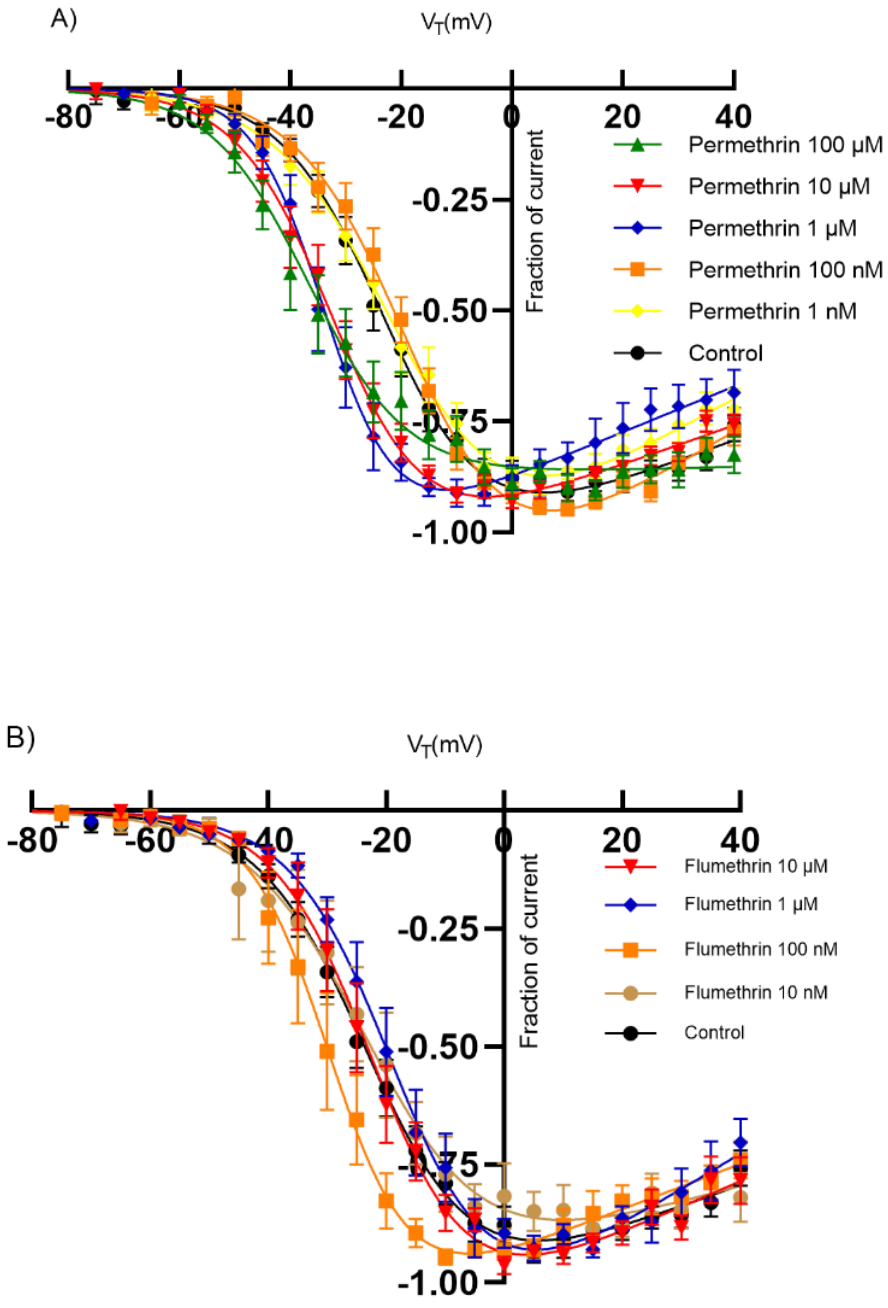

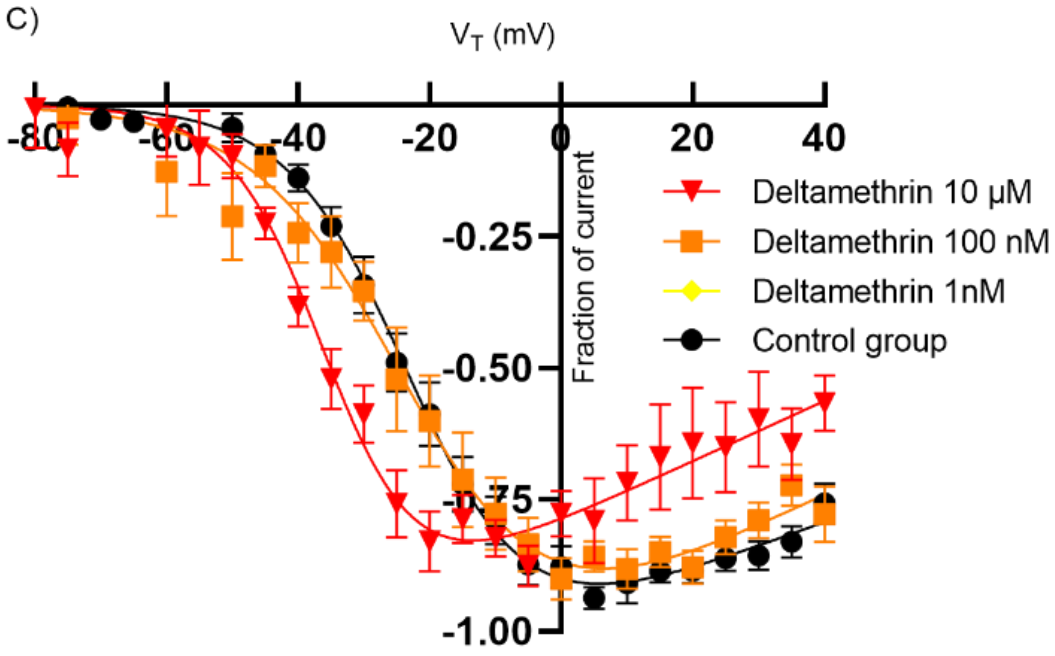

Figure 3.4: Influence of Pyrethroids on the Current-Voltage Characteristics of TE671 Voltage-Gated Na^+ Channels Using Voltage Protocol 1. A) Permethrin; B) Flumethrin; C) Deltamethrin. The graph displays the average normalized Na^+ currents with the fitted curves derived from Equation 1.

3.4.2 Effects of pyrethroids on activation

To elucidate the alterations in the voltage-dependence of human $Na_V1.7$ activation, we applied pyrethroids to TE671 cells and monitored the resultant Na^+ currents using Voltage Protocol 1. To evaluate the significance of observed changes, the extra-sum-of-squares F test was utilized. We administered pyrethroids at escalating concentrations ranging from 0.01 to 100 µM to assess their effects on the half-maximal activation voltage ($V_{50.act}$) of these cells.

Without the presence of any pyrethroid, the half-maximal activation voltage (V_{50}) was measured at -22.40 mV with a slope (K) of 10.01 mV.

When comparing this to treated samples, permethrin at higher concentration of 10 µM and 1 µM caused a significant hyperpolarizing shift in V_{50} to -32.22 ($p < 0.001$) mV and -33.09 ($p < 0.001$) mV, respectively. Conversely, at a concentration of 100 nM, the V_{50} value exhibited a significant depolarizing shift to -17.73 mV ($p < 0.001$). Moreover, at the lowest examined concentration of 1nM, a depolarizing effect was suggested by the V_{50}, although this did not reach statistical significance. The slope factor for $Na_v1.7$ activation by permethrin at 10 µM is 9.15 mV. At 1 µM, the slope factor is significantly reduced to 6.23 mV. At 100 nM, the slope factor is 9.71 mV, and at 1 nM, the value is 10.77 mV.

For flumethrin the V_{50} and slope factors were analysed at four distinct concentrations. At 10 µM, flumethrin showed a slight depolarizing shift in V_{50} to -21.37 mV. At a lower concentration of 1 µM, a more pronounced depolarizing shift was observed, with V_{50} significantly shifting to -17.43 mV ($p < 0.001$). In contrast, at 100 nM, the V_{50} significantly shifted in the hyperpolarizing direction to -29.16 mV ($p < 0.001$). The smallest concentration tested, 10 nM, resulted in a V_{50} of -22.58 mV, which does not significantly deviate from the control value, indicating a negligible effect on channel modulation at this concentration. The slope factors varied minimally across concentrations, with 10 µM at 8.45 mV, 1 µM at 8.67 mV, and 100 nM at 7.02 mV, increasing to 10.49 mV at 10 nM.

For deltamethrin, the V_{50} values at varying concentrations indicate distinct shifts. At 10 µM, deltamethrin causes a substantial hyperpolarizing shift in V_{50} to -37.28 mV ($p < 0.001$), which represents the most pronounced shift among the tested concentration. The slope factor at this concentration is 8.53 mV. At a lower concentration of 100 nM, the V_{50} shifts in the depolarizing direction to -22.6 mV. The corresponding slope factor at this concentration increases to 11.75 mV. At the lowest concentration of 1nM, the V_{50} is slightly depolarized to -23.35 mV, although this change is not statistically significant. The slope factor at this concentration is 9.95 mV, which is relatively close to the control slope value. Table 3.1 presents the comparative values of $V_{50.act}$ and slope factor (k) in TE671 cell $hNa_v1.7$ channels, comparing the presence and absence of pyrethroids.

A)

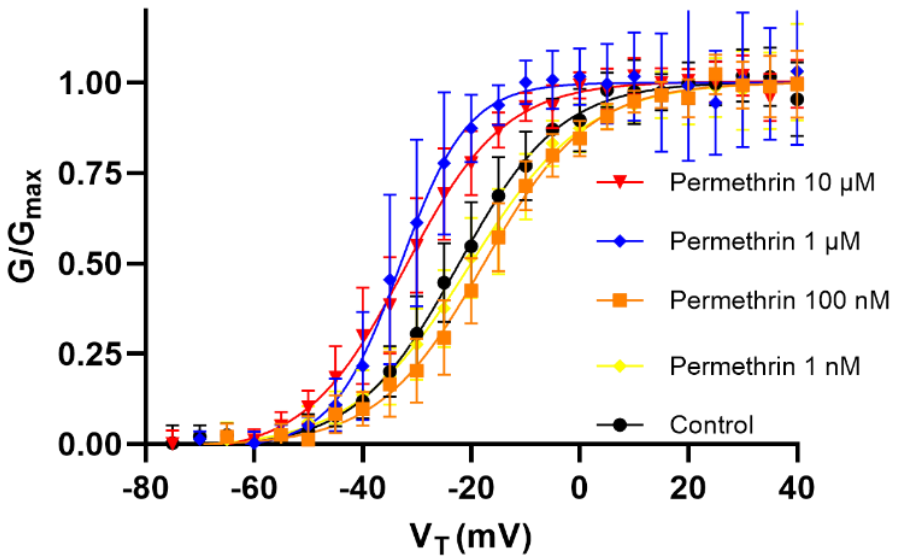
1.00
0.75
0.50
0.25
0.00
G/Gmax
-80
-60
-40
-20
0
20
40
VT (mV)
Permethrin 10 µM
Permethrin 1 µM
Permethrin 100 nM
Permethrin 1 nM
Control

B)

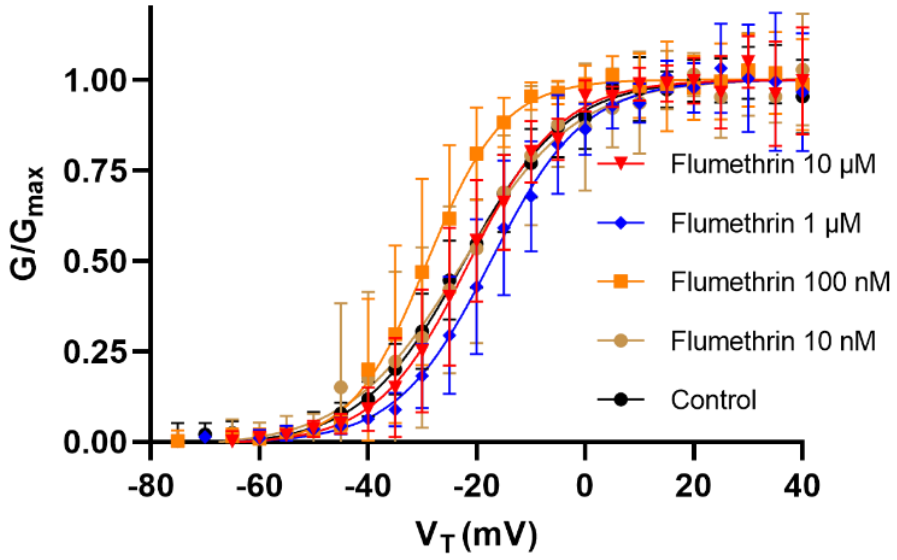
1.00
0.75
0.50
0.25
0.00
G/Gmax
-80
-60
-40
-20
0
20
40
VT (mV)
Flumethrin 10 µM
Flumethrin 1 µM
Flumethrin 100 nM
Flumethrin 10 nM
Control

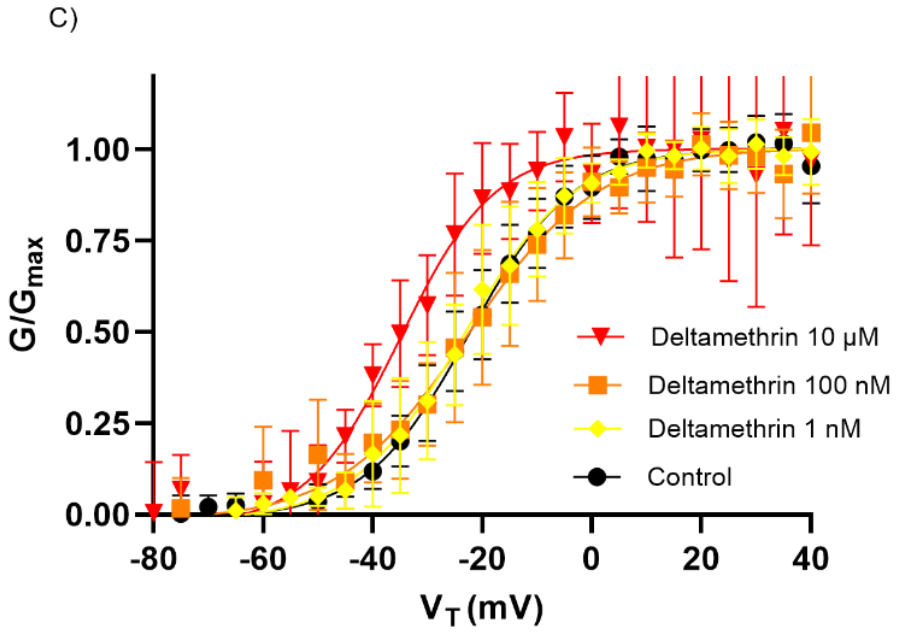

Figure 3.5: Impact of Escalating Pyrethroid Concentrations on the Conductance-Voltage Curves of TE671 Cell hNa$_V$1.7, Documented with Voltage Protocol 1, and Illustrated through Equation 3. A) Permethrin; B) Flumethrin; C) Deltamethrin.

Table 3.1: Comparative values of $V_{50.act}$ and Slope Factor (k) in TE671 Cell hNa$_V$1.7 Channels: Baseline versus Pyrethroid Exposure. *(P<0.001) (the values are derived from curve fitting to mean normalised current versus activation voltage)**

Pyrethroid	Concentration	$V_{50.act}$ (mV)	Slope, K (mV)	n
No pyrethroid		-22.40	10.01	15
Permethrin	10 µM	-32.22***	9.15	16
	1 µM	-33.09***	6.23	9
	100 nM	-17.73***	9.71	13
	1 nM	-20.24	10.77	23
Flumethrin	10 µM	-21.37	8.45	12
	1 µM	-17.43***	8.67	8
	100 nM	-29.16***	7.02	10
	10 nM	-22.58	10.49	8
Deltamethrin	10 µM	-37.28***	8.53	8
	100 nM	-22.6	11.75	8
	1 nM	-23.35	9.95	12

3.4.3 Effects of Pyrethroids on Inactivation

The effects of pyrethroids on the fast inactivation of the $hNa_v1.7$ were examined. The pyrethroids in various concentrations were tested on TE671 cells. The voltage-dependence of steady-state fast-inactivation was examined using protocol shown in Figure 2.2. To evaluate the significance of observed changes, the extra-sum-of-squares F test was utilized.

None of the tested pyrethroids caused statistically significant shift in the fast inactivation curve.

For permethrin the V_{50} shifted positively at 10 µM (-77.83 mV), 1 µM (-87.45 mV), 100 nM (-82.55 mV), and 1 nM (-78.73 mV), while a notable negative shift was observed at the highest concentration of 100 µM with a V_{50} of -99.5 mV.

For flumethrin positive shifts were recorded at 10 µM (-82.44 mV), 100 nM (-85.10 mV), 10 nM (-83.63 mV), and 1 nM (-81.45 mV), indicating prolonged channel opening and delayed inactivation. Contrastingly, negative shifts were observed at concentrations of 100 µM and 1 µM with V_{50}s of -100.80 mV and -90.40 mV, respectively, which suggests that at these concentrations, flumethrin facilitates channel inactivation at more hyperpolarized potentials.

Lastly, deltamethrin at both tested concentrations of 100 nM (-83.15 mV) and 1 nM (-78.95 mV) consistently caused a positive shift in the V_{50}, in line with permethrin's lower concentrations, thereby suggesting a delay in channel inactivation and prolonged sodium influx. Table 3.2 presents the comparative values of $V_{50.inact}$ and slope factor (k) in TE671 cell $hNa_v1.7$ channels, comparing the presence and absence of pyrethroids.

A)

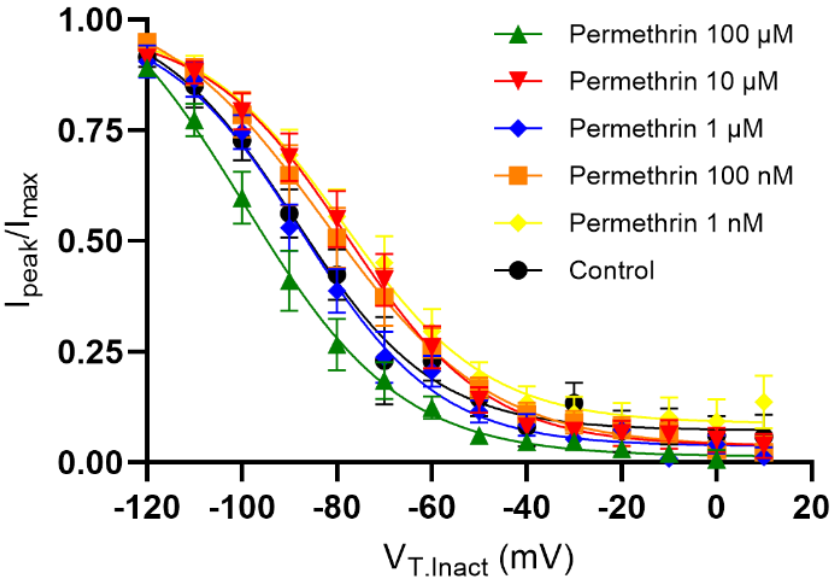
1.00
0.75
0.50
0.25
0.00
I_{peak}/I_{max}
-120
-100
-80
-60
-40
-20
0
20
$V_{T.Inact}$ (mV)
Permethrin 100 µM
Permethrin 10 µM
Permethrin 1 µM
Permethrin 100 nM
Permethrin 1 nM
Control

B)

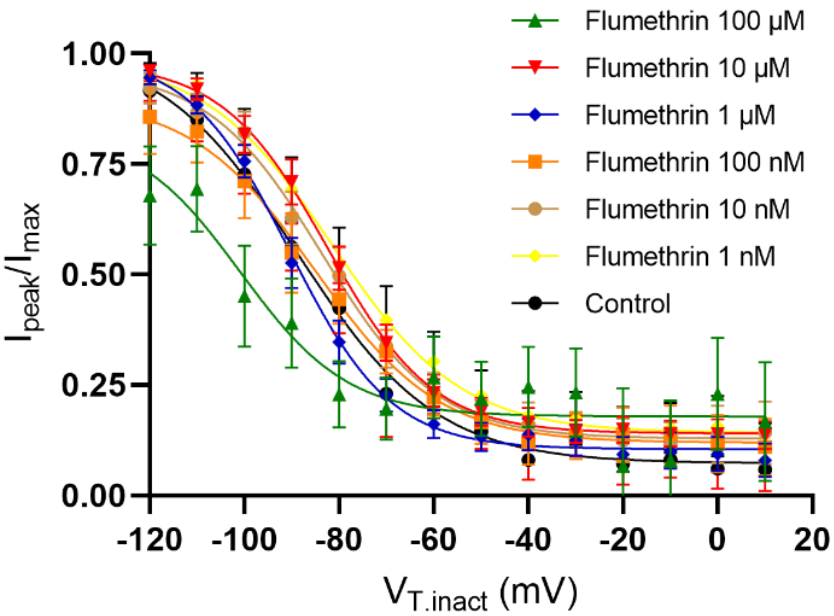
1.00
0.75
0.50
0.25
0.00
I_{peak}/I_{max}
-120
-100
-80
-60
-40
-20
0
20
$V_{T.inact}$ (mV)
Flumethrin 100 µM
Flumethrin 10 µM
Flumethrin 1 µM
Flumethrin 100 nM
Flumethrin 10 nM
Flumethrin 1 nM
Control

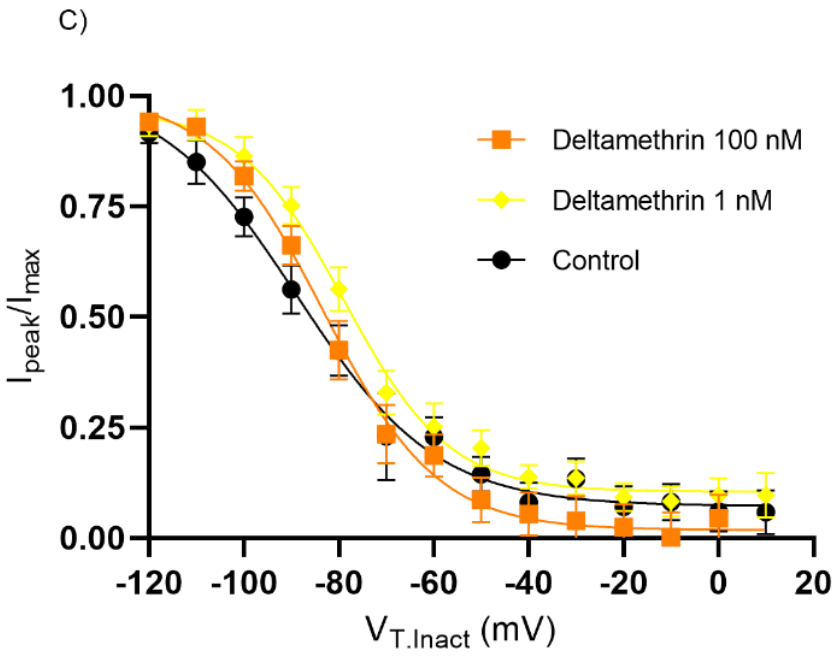

Figure 3.6: Influence of Elevated Pyrethroid Concentrations on the Voltage-Dependent Steady-State Fast Inactivation of TE671 Cell Voltage-Gated Na^+ Channels, Analyzed through Voltage Protocol 2 and Modelled with Equation 4. A) Permethrin; B) Flumethrin; C) Deltamethrin.

Table 3.2: Values of $V_{50.inact}$ of TE671 cell $Na_V1.7$ in the absence and presence of pyrethroids. (the values are derived from curve fitting to mean normalised current versus inactivation prepulse voltage)

Pyrethroid	Concentration	$V_{50.inact}$	Slope, K (mV)	n
No pyrethroid		-88.83	-14.66	23
Permethrin	100 µM	-99.5	-16.50	15
	10 µM	-77.83	-14.88	20
	1 µM	-87.45	-14.50	23
	100 nM	-82.55	-17.51	18
	1 nM	-78.73	-15.24	24
Flumethrin	100 µM	-100.80	-11.31	16
	10 µM	-82.44	-11.17	17
	1 µM	-90.40	-10.70	18
	100 nM	-85.10	-13.15	20
	10 nM	-83.63	-12.15	17
	1 nM	-81.45	-13.60	11
Deltamethrin	100 nM	-83.15	-11.97	13
	1 nM	-78.95	-11.04	14

3.4.4 Tail currents

The tail current phenomenon is a measurable effect that occurs when pyrethroids bind to the active voltage-gated Na^+ channels. This binding results in a delay of channel inactivation and deactivation, leading to prolonged sodium ion flow. These tail currents appear as sustained or slowly decaying currents following the repolarization phase of an action potential.

Mechanistically, pyrethroids stabilize the open state of the Na^+ channels, preventing them from closing promptly after activation. This stabilization prolongs the depolarized state of the membrane, resulting in sodium influx. The delayed inactivation increases the duration of the tail current, which can be observed as an extended current trace following the initial peak current in electrophysiological recordings.

In our study, we observed that only deltamethrin and flumethrin induced tail currents in voltage-gated Na^+ channels of TE671 cells, as depicted in Figure 3.7. These compounds modulated the channels in a concentration-dependent manner, with higher concentration of pyrethroids enhancing the amplitude of tail currents and decelerating their return to baseline. Each of these substances generated a pronounced tail current that subsided within 3-4 second after repolarization. Using the tail current amplitude immediately after repolarization, we estimated the percentage of maximum modification (M%) of Na^+ conductance in the presence of the pyrethroids, applying Equation 5. In the analysis of channel modulation, flumethrin exhibited a concentration-dependent integral modification of the voltage-gated Na^+ channels. This relationship was characterized by a progressive enhancement in channel modification with increasing concentrations of flumethrin, indicative of a dose-responsive alteration in channel kinetics.

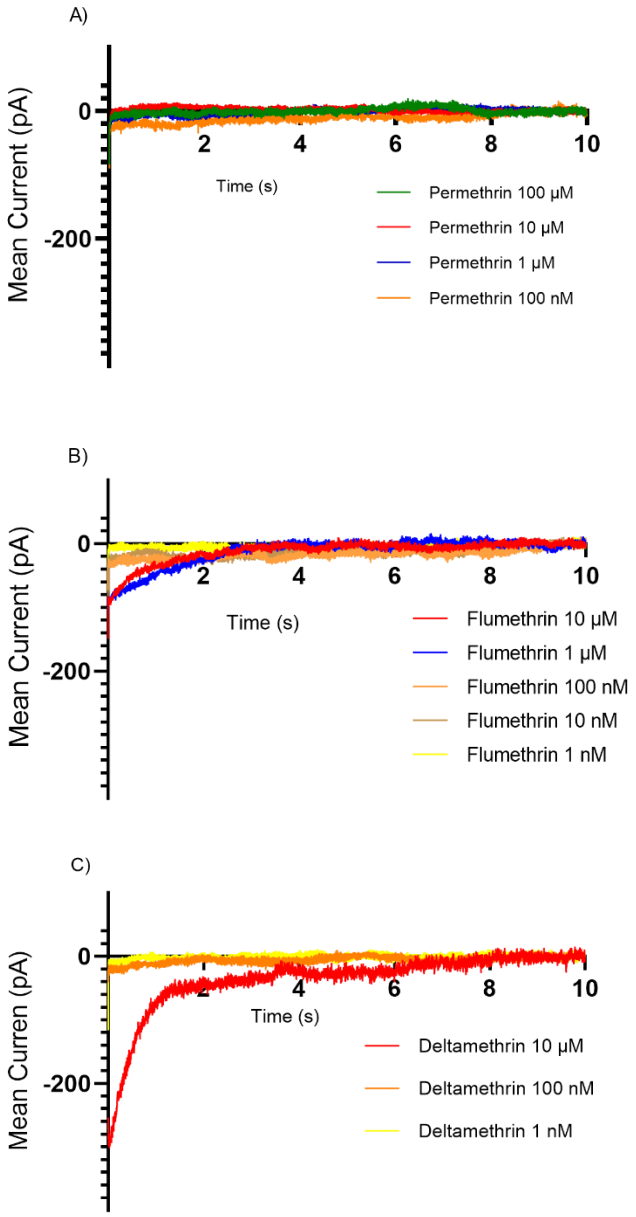

Figure 3.7: Tail Currents in TE671 Cells with and without Pyrethroid Treatment: A) Permethrin; B) Flumethrin; C) Deltamethrin. Tail currents were elicited using Voltage Protocol 6.

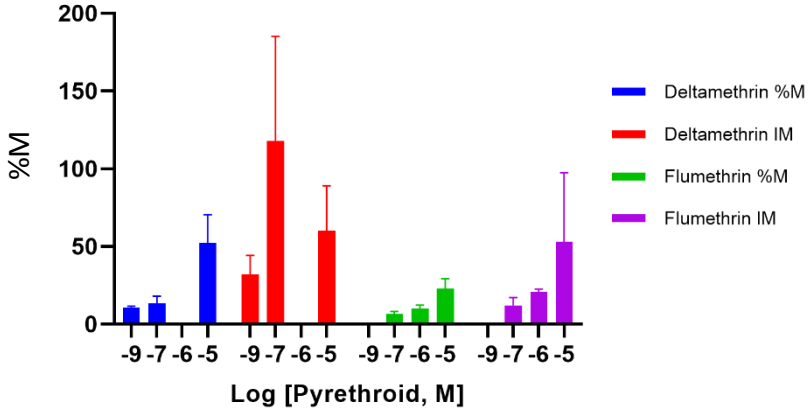

Figure 3.8: Concentration-response relationships for tail currents induced by deltamethrin and flumethrin in TE671 cells. The figure illustrates the combined sigmoidal log concentration-response curves, representing the tail current amplitudes as a percentage of the maximum modification potential (%M) for both deltamethrin and flumethrin on Na^+ channels. Additionally, the integrated modification (IM) analysis, which encompasses both the duration and amplitude of the tail currents, is plotted to demonstrate the extent of channel modification across different pyrethroid concentrations. Flumethrin: (10 µM, n=5); (1 µM , n=5); (100 nM, n=3), Deltamethrin: (10 µM, n=3); (100 nM, n=4); (1nM, n=4)

4 Discussion

Permethrin, a type I pyrethroid, at elevated concentrations, notably induced a hyperpolarizing shift in the V_{50} of activation, enhancing the channel's sensitivity to opening. Interestingly, permethrin uniquely did not elicit any tail currents across the tested concentrations, indicating a distinct mode of interaction with the $Na_v1.7$ channel compared to the other pyrethroids in this study. Flumethrin, a type II pyrethroid, demonstrated a concentration-dependent bidirectional modulation of $Na_v1.7$ activation. At 1 μM, a significant depolarizing shift was observed, indicating a reduced likelihood of channel opening at normal physiological voltages, whereas at 100 nM a hyperpolarizing shift was noted, thereby increasing the channel's sensitivity to opening. Furthermore, flumethrin induced tail currents, highlighting its capability to prolong channel activation or delay closure in a concentration-dependent manner. Deltamethrin, a type II pyrethroid, at a concentration of 10 μM, significantly shifted the V_{50} of activation towards hyperpolarization, thereby augmenting the channel's opening sensitivity. Like flumethrin, deltamethrin was found to produce tail currents, suggesting extended channel activation or delayed inactivation, which may underpin its neurotoxic effects. Across the range of pyrethroids and concentrations tested, none induced a significant change in the V_{50} of fast inactivation. This finding suggests that the neurotoxic potential of pyrethroids may predominantly arise from their ability to alter the activation threshold and sustain channel opening, rather than affecting the voltage dependence of the fast inactivation process.

Previous studies were focused on rat $Na_v1.2$, $Na_v1.3$, $Na_v1.6$, $Na_v1.7$ and $Na_v1.8$ expressed heterologously in Xenopus oocytes (62, 72-78). In this study, we investigated how deltamethrin, flumethrin, and permethrin affect the $Na_V1.7$ isoform of the human voltage-gated sodium channel, which is naturally present in TE671 cells. The $Na_v1.7$ isoform is TTX-S and expressed in the adult DRG neurons. Tetrodotoxin-resistant (TTX-R) Na^+ channels, which include $Na_v1.5$, $Na_v1.8$, and $Na_v1.9$, were previously found to be more responsive to allethrin compared to tetrodotoxin-sensitive (TTX-S) Na^+ channels, which are $Na_v1.1$, $Na_v1.2$, $Na_v1.3$, $Na_v1.4$, $Na_v1.6$, and $Na_v1.7$ (79). This indicates a differential sensitivity of Na^+ channel subtypes to allethrin, suggesting that the insecticide might preferentially target specific channels

within the neuronal membrane (80). Here, the sensitivity of the human TTX-sensitive $Na_V1.7$, when expressed in TE671 cells, to pyrethroids presents a striking contrast to the results obtained from previous research on TTX-resistant channels. Specifically, TTX-resistant channels such as $Na_V1.8$ and $Na_V1.9$, primarily involved in pain signal conduction in peripheral neurons, have been shown to be more responsive to pyrethroid compounds.

Permethrin, categorized as a Type I pyrethroid, induces the T intoxication syndrome in mammals following ingestion, whereas deltamethrin and flumethrin, which are Type II pyrethroids, lead to the development of CS syndrome in rodents (81). This chemical alteration not only enhances the potency of Type 2 pyrethroids but also fundamentally alters their mode of action compared to their Type 1 counterparts, which lack this cyano moiety. The presence of the cyano group contributes to a more pronounced neurotoxic effect on the nervous system of insects, disrupting sodium channel function more effectively and leading to rapid incapacitation and death of the target pests (82).

Type I and Type II pyrethroids influenced the voltage-dependent activation of $Na_V1.7$ channels in TE671 cells. Notably, exposure to permethrin, as well as elevated concentrations of deltamethrin and a specific 100 nM dose of flumethrin, was observed to induce considerable negative shifts in $V_{50.act}$. Among the pyrethroids tested, permethrin was the most effective in causing this specific change in channel behaviour. This negative displacement suggests a gain-of-function phenotype for the $Na_V1.7$ channels in the TE671 cellular model. The observed hyperpolarizing shift in the $V_{50.act}$ is significant as it predisposes the $Na_v1.7$ channels to a state of hyperexcitability by facilitating their activation at membrane potentials closer to the resting state. This heightened sensitivity and ease of activation may shed light on the mechanisms that drive pain perception. A relevant parallel can be drawn with Inherited Erythromelalgia (IEM), a pain disorder associated with mutations in the SCN9A gene, which encodes the $Na_V1.7$ channel. IEM mutations cause a negative shift in the activation of $Na_V1.7$ channels, similar to the effects observed with pyrethroid exposure in this study. This shift leads to increased excitability of sensory neurons,

providing a plausible explanation for the intense pain experienced by individuals with IEM, as their neurons are more easily triggered to send pain signals (83).

Deltamethrin and flumethrin induced tail currents that exhibited a slow decay, a characteristic commonly observed with other type II pyrethroids (84). Both Types I and II pyrethroids can induce tail currents in sodium channels but those induced by type II are much longer in duration, a key indicator of how these insecticides modify channel function. In experiments with Xenopus oocytes, these tail currents can be elicited through either a single long depolarization or multiple short depolarizations. The method used provides insights into the pyrethroids' effects on sodium channels in different states: resting or open. Type I pyrethroids, like cismethrin, effectively induce tail currents with a single prolonged depolarization, targeting channels in a resting or inactivated state. In contrast, Type II pyrethroids, such as deltamethrin and cypermethrin, require repeated depolarizations to affect sodium channels, typically binding to the channels in their open state. Although sequences of depolarizing pulses can enhance tail currents for Type I pyrethroids, this is not always the case, as seen with $rNa_v1.8$ channels treated with permethrin, which do not show increased tail currents after repeated stimulation. This highlights the complex interaction between pyrethroids and sodium channel dynamics (85). Paraesthesia in sensory neurons is thought to be triggered by sustained tail currents and a hyperpolarizing shift in activation within the voltage-gated sodium channels, leading to an increased susceptibility to Type II over Type I pyrethroids. This differential sensitivity is further validated by data from human occupational exposure studies (86) and research employing animal models (87), both of which illuminate the more pronounced effects of Type II pyrethroids. A study by Flannigan and Tucker (1985) specifically noted that the occurrence and intensity of paraesthesia in human volunteers due to permethrin exposure were notably less than those observed with cypermethrin, fenvalerate, and flucythrinate. Similarly, research by Cagen et al. (1984) on guinea pigs showed that responses to permethrin were significantly less intense than those elicited by Type II pyrethroids, including cypermethrin, deltamethrin, esfenvalerate, flucythrinate, and fenvalerate. Together, these studies emphasize the varied impacts of different

pyrethroids on both human and animal systems, especially highlighting permethrin's relatively lower neurotoxicity.

In this study, the differential effects of flumethrin, permethrin, and deltamethrin on the fast inactivation V_{50} of $Na_v1.7$ channels in the TE671 cell line were characterized by both hyperpolarizing and depolarizing shifts across a spectrum of concentrations. Intriguingly, these shifts did not achieve statistical significance when contrasted with the control, indicating that within the scope of the tested conditions, the alterations in channel gating induced by the pyrethroids were not distinct from natural cellular variability. Our experimental findings resonate with previously established research on the pharmacological properties of the rat $Na_V1.7$ voltage-gated sodium channel, particularly reflecting the work of Tan and Soderlund (2011). In their study, conducted using a Xenopus oocyte expression system, the impact of tefluthrin, a Type I pyrethroid, on $Na_V1.7$ channels was assessed. They discovered that at a concentration of 100 µM, tefluthrin did not markedly alter the voltage dependence of either peak sodium current activation or the steady-state fast inactivation. This observation implies that tefluthrin, despite affecting the inactivation kinetics, does not significantly modify the voltage threshold for channel activation or inactivation, thereby preserving the channel's voltage responsiveness despite changes in kinetics. Our observations, while aligning with these findings regarding inactivation, diverge when it comes to activation effects. This discrepancy could hint at the influence of beta subunits, which might not have been present in Tan and Soderlund's experimental setup. Considering that beta subunits are likely expressed in TE671 cells, their presence could account for the observed differences in channel activation. This suggests that the interaction between tefluthrin and the $Na_V1.7$ channel, particularly in terms of activation, could be modulated by components such as beta subunits, which were not accounted for in the earlier study, providing a potential avenue for further exploration into the mechanistic differences observed (88). The study conducted by Tan and Soderlund (2011) reported that exposure to 100 µM tefluthrin, a Type I pyrethroid, led to a prolongation of channel inactivation and the emergence of late current, as well as rapidly decaying tail currents in rat $Na_V1.7$ channels expressed in Xenopus oocytes. Although the study found these effects of tefluthrin

on $Na_v1.7$ channels, it also noted that $Na_v1.7$ exhibited lower sensitivity to tefluthrin compared to other sodium channel isoforms like $Na_v1.3$ and $Na_v1.6$ when tested under similar conditions. This reduced sensitivity contributes to the complexity of understanding pyrethroid actions in the peripheral nervous system, where Nav1.7 channels are predominantly expressed (88). Contrary to Tan & Soderlund (2011), our study employing a comparable concentration of permethrin, another Type I pyrethroid, did not elicit similar decaying tail currents in the $Na_V1.7$ channel. This discrepancy highlights a potentially selective interaction between different Type I pyrethroids and the $Na_V1.7$ sodium channel, suggesting that structural variations within this class of compounds could lead to divergent electrophysiological outcomes. Our findings, therefore, contribute to a nuanced understanding of pyrethroid-channel interactions, underlining the necessity for isoform-specific studies to ascertain the molecular determinants of channel modulation by various pyrethroid compounds. Wolansky et al. (2006) suggest that the reason tefluthrin induces tail current could be its high potency, comparable to that of deltamethrin and surpassing that of other Type I pyrethroids like permethrin, resmethrin, bifenthrin, and S-bioallethrin (89). Additionally, Choi & Soderlund (2006) found tefluthrin to be one of the most potent substances among 11 pyrethroids tested on rat $Na_V1.8$. They indicated that tefluthrin, alongside cismethrin, allethrin, and permethrin, modified the sodium channels in a way that they activate quickly and inactivate only partially within the timeframe of the depolarization used in this study. Moreover, when considering the effectiveness of these compounds in terms of resting or use-dependent modification, tefluthrin was noted to approach the potency of fenpropathrin, which was identified as the most effective compound against $Na_V1.8$ channels in the study by (72).

The 2020 study by Thull et al. provides significant insights into the effects of the pyrethroid deltamethrin on human sodium channels, specifically $Na_v1.5$ and $Na_v1.7$, using whole-cell patch clamp techniques on mammalian cells. This study is highly relevant to understanding the broader implications of pyrethroid interactions with human sodium channels. Thull et al. (2020) demonstrate that deltamethrin induces resurgent-like tail currents in human cardiac $Na_v1.5$ channels. These currents are characterized by a distinct hooked appearance, which is observed during

repolarization following a depolarizing voltage step. The study reveals that deltamethrin significantly slows both fast inactivation and deactivation of $Na_v1.5$ channels, leading to large persistent currents. This is critical because the altered kinetics suggest a substantial impact on the channel's normal gating behavior, potentially leading to abnormal cardiac excitability and arrhythmias. Furthermore, the study extends its analysis to $Na_v1.7$ channels, where 1 μM deltamethrin also induced tail currents, albeit much smaller than those observed with $Na_v1.5$. This finding is noteworthy because it indicates that while $Na_v1.5$ is more significantly affected, $Na_v1.7$ also exhibits sensitivity to deltamethrin, which could have implications for sensory neurons where $Na_v1.7$ is predominantly expressed. The study suggests that the presence of deltamethrin modifies the gating states of Na_v channels, creating additional conductive states that contribute to the observed hooked resurgent-like currents. The sea anemone toxin ATx-II was used to confirm these findings by preventing fast inactivation-related processes, thereby eliminating resurgent-like currents while preserving persistent currents. This indicates that the induction of resurgent-like currents by deltamethrin is dependent on the interplay between fast inactivation and deactivation kinetics (90).

Soderlund et al. (2017) presents a comprehensive analysis of the interaction between pyrethroids and the rat $Na_V1.6$ sodium channel, both in its native form and when expressed in heterologous systems such as Xenopus oocytes and HEK293 cells. In Xenopus oocytes, deltamethrin and tefluthrin had a minimal effect, with the most notable effects was a slight increase in the proportion of channels resistant to inactivation following depolarization. Conversely, in HEK293 cells, both tefluthrin and deltamethrin induced significant hyperpolarizing shifts in the voltage-dependence of channel activation and inactivation. In Xenopus oocytes, modification of $Na_V1.6$ channels by deltamethrin predominantly required repetitive depolarization, suggesting a preference for binding to open channels. Tefluthrin, however, modified resting $Na_V1.6$ channels and exhibited enhanced modification upon repeated depolarization, indicating its ability to bind both resting and open $Na_V1.6$ channels. Conversely, in HEK293 cells, both tefluthrin and deltamethrin induced noticeable modifications in resting states of $Na_V1.6$ channels, with deltamethrin's modification

further enhanced by repeated depolarization. The auxiliary β subunits, particularly β1, are essential for the use-dependent modification of $Na_V1.6$ channels by pyrethroids in Xenopus oocytes. The inclusion of β2 subunit did not further alter the modification effects induced by the β1 subunit. This pattern of subunit necessity for pyrethroid modification was observed not only for $Na_V1.6$ but also for the rat $Na_V1.3$ sodium channel isoform. In HEK293 cells, the presence of β subunits was necessary to observe use-dependent enhancement of $Na_V1.6$ channels' modification by deltamethrin, specifically requiring the β2 subunit for these use-dependent effects (91).

Tan and Soderlund (2009) showed that tefluthrin caused the $V_{50.act}$ to move closer to the depolarizing potential in both rat and human $Na_V1.3$ channels without affecting the inactivation's voltage-dependency. Additionally, they observed that tefluthrin decelerated the activation, inactivation, and deactivation kinetics of $Na_V1.3$ channels in both species and induced the generation of tail currents. For both rat and human channels, tefluthrin modification led to prolonged τ_{fast} and τ_{slow} components of inactivation across a range of test potentials. This modification increased the proportion of channels exhibiting slow inactivation kinetics, indicating a significant impact on channel behaviour that could affect neuronal excitability and signalling. The analysis also highlighted species differences in sensitivity to tefluthrin, with rat $Na_V1.3$ channels showing approximately four-fold greater modification by tefluthrin compared to human $Na_V1.3$ channels under resting conditions. This differential sensitivity suggests that despite the high degree of amino acid sequence conservation between rat and human sodium channel isoforms, there are functional differences in how these channels respond to pyrethroid insecticides. The observation that tefluthrin does not alter the voltage-dependence of the inactivation process for $hNa_V1.3$ channels, as reported in the study, aligns with the outcomes of our experiments on $Na_V1.7$ channels in human TE671 cells. In their research, the observation that tefluthrin induces tail currents and incomplete inactivation in both rat and human $Na_V1.3$ channels highlights a pivotal mechanism by which pyrethroids manifest their neurotoxic properties (76).

Smith & Soderlund (2001) detailed that cypermethrin, a Type II pyrethroid, significantly shifted the activation voltage-dependence of rat $Na_V1.8$ channels towards hyperpolarization. Similarly, cismethrin, a Type I pyrethroid, induced a hyperpolarizing shift, consistent with our results. In contrast, both pyrethroids caused a notable depolarizing shift in the voltage-dependence of inactivation for rat $Na_V1.8$, diverging from our findings (74). Smith and Soderlund (2001) indicate that $Na_V1.7$ channels, abundantly found in dorsal root ganglion (DRG) neurons, significantly contribute to the tetrodotoxin-sensitive (TTX-S) voltage-gated Na^+ currents that are not affected by pyrethroids. This conclusion is based on the observation that DRG neurons contain both TTX-sensitive and TTX-resistant types of sodium channels, with the latter being more prone to alterations by pyrethroids. Therefore, the existence of a current in DRG neurons that is unaffected by pyrethroids among the TTX-sensitive channels suggests the involvement of $Na_V1.7$ channels. These channels are noted for their prevalence in DRG neurons and their sensitivity to TTX (74).

The research by Vais et al. (2000) identified that a substitution of isoleucine for methionine at position 874 (equivalent to the super-kdr site 918 in the housefly) in the rat $Na_V1.2$ sodium channel alpha subunit resulted in a 100-fold increase in sensitivity to the pyrethroid insecticide deltamethrin, with a focus on whole-cell electrophysiological measurements. This single amino acid change parallels mutations observed in pyrethroid-resistant houseflies, suggesting a common structural basis for pyrethroid sensitivity across species. The study proposes that this specific residue difference might account for the lower pyrethroid sensitivity observed in mammalian channels compared to their insect counterparts (77).

The amino acid at position 918 is a critical determinant of the species-selectivity of pyrethroids. Many studies have highlighted its importance, and one key paper by Usherwood et al. (2007) further elucidates this role. Usherwood et al. investigated mutations in DIIS5 and the DIIS4-S5 linker of the Drosophila melanogaster sodium channel, demonstrating that the M918T mutation significantly decreases sensitivity to deltamethrin and permethrin while slightly increasing sensitivity to fenfluthrin. This study suggests that the absence of the second aromatic ring in fenfluthrin contributes to this differential sensitivity. Given that tefluthrin is a close analogue of

fenfluthrin, the findings by Usherwood et al. are highly relevant. The observed effects of tefluthrin can be better understood in light of these findings, as the fluorinated aromatic ring and structural analogies with fenfluthrin likely influence its binding and action on sodium channels (92).

In their comprehensive study, Peng et al. (2009) meticulously investigate the electrophysiological ramifications of deltamethrin exposure on both wild-type (WT) and I874M mutant (M874) $Na_V1.2$ sodium channels, expressed in Xenopus oocytes. This research not only examines the fundamental properties such as channel lifetimes and opening probabilities but also sheds light on how deltamethrin influences these parameters. A key finding from their work is the compelling evidence suggesting that pyrethroids are capable of binding to and modulating sodium channels primarily in their open state. This conclusion is drawn from the observation that, in the presence of deltamethrin, the distribution of channel open times transitions from being best described by single exponentials (in the absence of the insecticide) to two exponentials. This indicates the emergence of two distinct populations of channel openings: one that remains unaffected by the insecticide and another that experiences significant prolongation. Such bifurcation is indicative of deltamethrin's action in extending the open states of the $Na_V1.2$ channels. Furthermore, the study elucidates how the I874M mutation amplifies the sensitivity of the channels to deltamethrin. Remarkably, it was observed that a lower concentration of deltamethrin was required to influence the M874 channels as compared to their WT counterparts, highlighting the mutation's role in enhancing channel sensitivity to pyrethroids. This mutation-specific sensitivity offers profound insights into the interaction dynamics between pyrethroids and sodium channels, suggesting that the local structural configuration around the I874M mutation may facilitate a higher affinity interaction or modify the interaction dynamics between the channel and pyrethroid molecules (93). The human $Na_v1.2$ possesses an isoleucine (I) residue in place of methionine (M), with neighbouring amino acids showing high conservation across various mammalian subtypes. This suggests that alternate sites could contribute to its sensitivity.

Before the research conducted by Tan and Soderlund in 2011, $Na_V1.2$ was recognized as the sole pyrethroid-resistant isoform in rats. The discovery of $Na_V1.7$ as another isoform resistant to pyrethroids opened avenues for exploring the differences in amino acid sequences that distinguish channels as either sensitive or resistant to pyrethroids. By comparing the sequences of four sensitive isoforms (house fly Vssc1, and rat $Na_V1.3$, $Na_V1.6$, and $Na_V1.8$) with two resistant isoforms (rat $Na_V1.2$ and $Na_V1.7$), a unique site was identified where the sequences diverged between sensitive and resistant types. This site, in the transmembrane segment 6 of domain I, features a valine in sensitive isoforms and an isoleucine in resistant ones, located in a highly conserved region thought to be part of the inner pore. Interestingly, this valine site has been linked to pyrethroid resistance in insects through various mutations, indicating its critical role. Although this polymorphism is a key factor in determining pyrethroid sensitivity among rat sodium channel isoforms, it's not the sole determinant, as evidenced by differences in pyrethroid sensitivity between rat and human $Na_V1.3$ channels that share the valine residue. This suggests that other factors influencing differential sensitivity among mammalian sodium channel isoforms are yet to be identified (88).

The discovery of a multitude of mutations linked to resistance (known as kdr and super-kdr) within insect sodium channels has offered significant clues towards pinpointing the pyrethroid binding sites on both insect and human sodium channels. The cumulative body of evidence indicates that pyrethroids interact with the α-subunit of the voltage-gated sodium channel (6, 94). Mutations in the α-subunit associated with resistance are most frequently observed in the domain II region of the sodium channel. These mutations, particularly in the DIIS6 segment, are linked to knockdown resistance (kdr), including the L1014F, L1014H, and L1014S mutations. In addition, mutations in the DIIS5 segment (T929I) and the DIIS4-S5 linker (M918T) are associated with super-kdr resistance. Other mutations contributing to resistance have been found in the S6 transmembrane segments of domains I and III (95). Electrophysiological studies on kdr mutant channels in oocytes are utilized to measure the impact of kdr mutations on channel gating mechanisms and pyrethroid binding affinity. Vais et al. (2000a) demonstrated that the kdr mutation (L1014F) in the DIIS6

segment and the super-kdr mutations M918T in the DIIS4–S5 linker and T929I in DIIS5 all led to an increase in closed-state inactivation. This, in turn, decreased the frequency of channel openings, a process necessary for pyrethroid activity. Moreover, these mutations were found to lower the binding affinity for the channels when they are in their open state (77, 96). Meanwhile, substitution of isoleucine to methionine at position 780 in the DIIS4-S5 linker in the rat $Na_V1.8$ increased the sensitivity of $Na_V1.8$ to cismethrin (75). O'Reilly et al. (2006) provided a compelling model suggesting that pyrethroids exhibit a preference for targeting the open conformation of voltage-gated Na^+ channels, specifically interacting with key amino acids located in the domain II S4-S5 linker (notably M918) and within the IIS5 and IIIS6 helices. This framework not only underscores the critical roles of the IIS4–S5 linker and the IIS5 and IIIS6 helices in facilitating pyrethroid binding but also confirms the involvement of specific residues — M918, T929, and F1519 — as integral to this binding process. Furthermore, the model proposes the presence of additional residues within the IIS5 and IIIS6 segments that potentially contribute to the pyrethroid binding site. These findings suggest a structural basis for the observed variances in pyrethroid sensitivity between insect and mammalian sodium channels, offering insights into the molecular dynamics underpinning pyrethroid interactions with these channels (97). Based on what we understand, the $Na_V1.7$ isoform shares a common feature with other vertebrate voltage-gated sodium channel isoforms: it has a conserved isoleucine residue at the same sequence position (918) as found in insect sodium channels. These findings collectively underscore the critical role of residues in the DIIS4-S5 linker in defining the pyrethroid binding site of the $Na_V1.7$ channels in TE671 cells.

Exposure to pyrethroids may induce symptoms akin to those observed in cases of hereditary Inherited Erythromelalgia (IEM) and Paroxysmal Extreme Pain Disorder (PEPD), suggesting a pathogenesis closely linked to gain-of-function mutations within the $Na_V1.7$ channels of peripheral sensory neurons. Such mutations in $Na_V1.7$ channels, which play a crucial role in pain perception, lead to hyperexcitability of these channels, thereby enhancing pain sensitivity and triggering other associated symptoms. Moreover, individuals possessing these gain-of-function mutations in their $Na_V1.7$ channels, akin to those detected in patients with Inherited Erythromelalgia,

may exhibit an increased vulnerability to pyrethroid exposure. This elevated risk may stem from the synergistic effects of pyrethroids on pre-existing hyperactive $Na_V1.7$ channels, consequently amplifying the excitability of sensory neurons to symptomatic levels.

One significant point to discuss is the discrepancy in the observed reversal potential V_{rev} and the V_{50} of activation in our study compared to the findings by Ngum et al. (2022). Our study recorded a reversal potential of +210 mV, whereas Ngum et al. (2022) reported a more realistic value of approximately +70 mV. Additionally, the V_{50} of activation in our study was -22.4 mV compared to -31.9 mV in the Ngum et al. (2022) paper. One primary factor that could account for the difference in the reversal potential and V_{50} is the use of different models of amplifiers in the two studies. Amplifier calibration and settings can significantly impact the recorded reversal potentials and V_{50}. The Axopatch 200A used by Ngum et al. (2022) might have different calibration protocols or inherent characteristics compared to the amplifier used in our study. The inclusion of 1 mM CaCl in the pipette solution in our study might also have influenced the intracellular ionic environment, potentially affecting the recorded reversal potential and V_{50}. However, given the magnitude of the discrepancy, it is more plausible that the primary factor is the difference in amplifier models and their respective calibration settings.

References

1. Mariana Furio Franco B, Murilo P, Lilian Cristina P, Daniel Junqueira D. Impact of Pesticides on Environmental and Human Health. In: Ana Cristina A, Gustavo S, editors. Toxicology Studies. Rijeka: IntechOpen; 2015. p. Ch. 8.
2. Tudi M, Daniel Ruan H, Wang L, Lyu J, Sadler R, Connell D, et al. Agriculture Development, Pesticide Application and Its Impact on the Environment. Int J Environ Res Public Health. 2021;18(3).
3. Field LM, Emyr Davies TG, O'Reilly AO, Williamson MS, Wallace BA. Voltage-gated sodium channels as targets for pyrethroid insecticides. Eur Biophys J. 2017;46(7):675-9.
4. Casida JE. Pyrethrum flowers and pyrethroid insecticides. Environ Health Perspect. 1980;34:189-202.
5. Soderlund DM, Clark JM, Sheets LP, Mullin LS, Piccirillo VJ, Sargent D, et al. Mechanisms of pyrethroid neurotoxicity: implications for cumulative risk assessment. Toxicology. 2002;171(1):3-59.
6. Shafer TJ, Meyer DA, Crofton KM. Developmental neurotoxicity of pyrethroid insecticides: critical review and future research needs. Environ Health Perspect. 2005;113(2):123-36.
7. Chrustek A, Hołyńska-Iwan I, Dziembowska I, Bogusiewicz J, Wróblewski M, Cwynar A, et al. Current Research on the Safety of Pyrethroids Used as Insecticides. Medicina (Kaunas). 2018;54(4).
8. Ahamad A, Kumar J. Pyrethroid pesticides: An overview on classification, toxicological assessment and monitoring. Journal of Hazardous Materials Advances. 2023;10:100284.
9. Narahashi T. Neuronal ion channels as the target sites of insecticides. Pharmacol Toxicol. 1996;79(1):1-14.
10. Fujino C, Watanabe Y, Sanoh S, Nakajima H, Uramaru N, Kojima H, et al. Activation of PXR, CAR and PPARα by pyrethroid pesticides and the effect of metabolism by rat liver microsomes. Heliyon. 2019;5:e02466.
11. Burton MJ, Mellor IR, Duce IR, Davies TG, Field LM, Williamson MS. Differential resistance of insect sodium channels with kdr mutations to deltamethrin, permethrin and DDT. Insect Biochem Mol Biol. 2011;41(9):723-32.
12. Xu L, Ding X, Wang T, Mou S, Sun H, Hou T. Voltage-gated sodium channels: structures, functions, and molecular modeling. Drug Discovery Today. 2019;24(7):1389-97.
13. Catterall WA. Voltage gated sodium and calcium channels: Discovery, structure, function, and Pharmacology. Channels (Austin). 2023;17(1):2281714.
14. Wu Y, Ma H, Zhang F, Zhang C, Zou X, Cao Z. Selective Voltage-Gated Sodium Channel Peptide Toxins from Animal Venom: Pharmacological Probes and Analgesic Drug Development. ACS Chemical Neuroscience. 2018;9(2):187-97.
15. de Lera Ruiz M, Kraus RL. Voltage-Gated Sodium Channels: Structure, Function, Pharmacology, and Clinical Indications. Journal of Medicinal Chemistry. 2015;58(18):7093-118.
16. Marban E, Yamagishi T, Tomaselli GF. Structure and function of voltage-gated sodium channels. J Physiol. 1998;508 (Pt 3)(Pt 3):647-57.
17. Hodgkin AL, Huxley AF. The components of membrane conductance in the giant axon of Loligo. J Physiol. 1952;116(4):473-96.
18. Hodgkin AL, Huxley AF. Currents carried by sodium and potassium ions through the membrane of the giant axon of Loligo. J Physiol. 1952;116(4):449-72.
19. Hodgkin AL, Huxley AF. The dual effect of membrane potential on sodium conductance in the giant axon of Loligo. J Physiol. 1952;116(4):497-506.
20. Hodgkin AL, Huxley AF. A quantitative description of membrane current and its application to conduction and excitation in nerve. J Physiol. 1952;117(4):500-44.

21. Neher E, Sakmann B. Single-channel currents recorded from membrane of denervated frog muscle fibres. Nature. 1976;260(5554):799-802.
22. Beneski DA, Catterall WA. Covalent labeling of protein components of the sodium channel with a photoactivable derivative of scorpion toxin. Proc Natl Acad Sci U S A. 1980;77(1):639-43.
23. Agnew WS, Cooper EC, James WM, Tomiko SA, Rosenberg RL, Emerick MC, et al. Chapter 17 Voltage-Sensitive Sodium Channels: Molecular Structure and Function. In: Hoffman JF, Giebirch G, editors. Current Topics in Membranes and Transport. 33: Academic Press; 1988. p. 329-65.
24. Hartshorne RP, Catterall WA. Purification of the saxitoxin receptor of the sodium channel from rat brain. Proc Natl Acad Sci U S A. 1981;78(7):4620-4.
25. Hartshorne RP, Catterall WA. The sodium channel from rat brain. Purification and subunit composition. J Biol Chem. 1984;259(3):1667-75.
26. Hartshorne RP, Keller BU, Talvenheimo JA, Catterall WA, Montal M. Functional reconstitution of the purified brain sodium channel in planar lipid bilayers. Proc Natl Acad Sci U S A. 1985;82(1):240-4.
27. Noda M, Shimizu S, Tanabe T, Takai T, Kayano T, Ikeda T, et al. Primary structure of Electrophorus electricus sodium channel deduced from cDNA sequence. Nature. 1984;312(5990):121-7.
28. Brackenbury WJ, Isom LL. Na Channel β Subunits: Overachievers of the Ion Channel Family. Front Pharmacol. 2011;2:53.
29. Shen H, Zhou Q, Pan X, Li Z, Wu J, Yan N. Structure of a eukaryotic voltage-gated sodium channel at near-atomic resolution. Science. 2017;355(6328):eaal4326.
30. Zhang J, Mao W, Ren Y, Sun R-N, Yan N, Gong H. Simulating the ion permeation and ion selection for a eukaryotic voltage-gated sodium channel NaVPaS. Protein & Cell. 2018;9(6):580-5.
31. Labro AJ, Snyders DJ. Being Flexible: The Voltage-Controllable Activation Gate of Kv Channels. Frontiers in Pharmacology. 2012;3.
32. Long SB, Tao X, Campbell EB, MacKinnon R. Atomic structure of a voltage-dependent K+ channel in a lipid membrane-like environment. Nature. 2007;450(7168):376-82.
33. Horn R, Ding S, Gruber HJ. Immobilizing the Moving Parts of Voltage-Gated Ion Channels. Journal of General Physiology. 2000;116(3):461-76.
34. Pless SA, Elstone FD, Niciforovic AP, Galpin JD, Yang R, Kurata HT, et al. Asymmetric functional contributions of acidic and aromatic side chains in sodium channel voltage-sensor domains. Journal of General Physiology. 2014;143(5):645-56.
35. West JW, Patton DE, Scheuer T, Wang Y, Goldin AL, Catterall WA. A cluster of hydrophobic amino acid residues required for fast Na(+)-channel inactivation. Proc Natl Acad Sci U S A. 1992;89(22):10910-4.
36. Hartmann HA, Tiedeman AA, Chen SF, Brown AM, Kirsch GE. Effects of III-IV linker mutations on human heart Na+ channel inactivation gating. Circ Res. 1994;75(1):114-22.
37. Kellenberger S, West JW, Scheuer T, Catterall WA. Molecular analysis of the putative inactivation particle in the inactivation gate of brain type IIA Na+ channels. J Gen Physiol. 1997;109(5):589-605.
38. Goldin AL. Mechanisms of sodium channel inactivation. Curr Opin Neurobiol. 2003;13(3):284-90.
39. Pan X, Li Z, Zhou Q, Shen H, Wu K, Huang X, et al. Structure of the human voltage-gated sodium channel Na(v)1.4 in complex with β1. Science. 2018;362(6412).
40. Shen H, Liu D, Wu K, Lei J, Yan N. Structures of human Na(v)1.7 channel in complex with auxiliary subunits and animal toxins. Science. 2019;363(6433):1303-8.
41. Wu Q, Huang J, Fan X, Wang K, Jin X, Huang G, et al. Structural mapping of Nav1.7 antagonists. Nature Communications. 2023;14(1):3224.

42. Capes DL, Goldschen-Ohm MP, Arcisio-Miranda M, Bezanilla F, Chanda B. Domain IV voltage-sensor movement is both sufficient and rate limiting for fast inactivation in sodium channels. Journal of General Physiology. 2013;142(2):101-12.
43. Vilin YY, Ruben PC. Slow inactivation in voltage-gated sodium channels: molecular substrates and contributions to channelopathies. Cell Biochem Biophys. 2001;35(2):171-90.
44. Ahern CA, Payandeh J, Bosmans F, Chanda B. The hitchhiker's guide to the voltage-gated sodium channel galaxy. J Gen Physiol. 2016;147(1):1-24.
45. Catterall WA, Goldin AL, Waxman SG. International Union of Pharmacology. XXXIX. Compendium of Voltage-Gated Ion Channels: Sodium Channels. Pharmacological Reviews. 2003;55(4):575-8.
46. Yu FH, Catterall WA. Overview of the voltage-gated sodium channel family. Genome Biol. 2003;4(3):207.
47. Catterall WA, Goldin AL, Waxman SG. International Union of Pharmacology. XLVII. Nomenclature and structure-function relationships of voltage-gated sodium channels. Pharmacol Rev. 2005;57(4):397-409.
48. Waxman SG. Channel, neuronal and clinical function in sodium channelopathies: from genotype to phenotype. Nat Neurosci. 2007;10(4):405-9.
49. Dib-Hajj SD, Cummins TR, Black JA, Waxman SG. Sodium channels in normal and pathological pain. Annu Rev Neurosci. 2010;33:325-47.
50. Rush AM, Cummins TR, Waxman SG. Multiple sodium channels and their roles in electrogenesis within dorsal root ganglion neurons. J Physiol. 2007;579(Pt 1):1-14.
51. Simkin D, Bendahhou S. Skeletal muscle na channel disorders. Front Pharmacol. 2011;2:63.
52. Zimmer T, Benndorf K. The human heart and rat brain IIA Na+ channels interact with different molecular regions of the beta1 subunit. J Gen Physiol. 2002;120(6):887-95.
53. Catterall WA. Structure and function of voltage-gated sodium channels at atomic resolution. Exp Physiol. 2014;99(1):35-51.
54. Klugbauer N, Lacinova L, Flockerzi V, Hofmann F. Structure and functional expression of a new member of the tetrodotoxin-sensitive voltage-activated sodium channel family from human neuroendocrine cells. Embo j. 1995;14(6):1084-90.
55. Trombley P, Westbrook G. Voltage-gated currents in identified rat olfactory receptor neurons. The Journal of Neuroscience. 1991;11(2):435-44.
56. Herzog RI, Cummins TR, Ghassemi F, Dib-Hajj SD, Waxman SG. Distinct repriming and closed-state inactivation kinetics of Nav1.6 and Nav1.7 sodium channels in mouse spinal sensory neurons. J Physiol. 2003;551(Pt 3):741-50.
57. Cummins TR, Howe JR, Waxman SG. Slow closed-state inactivation: a novel mechanism underlying ramp currents in cells expressing the hNE/PN1 sodium channel. J Neurosci. 1998;18(23):9607-19.
58. Drenth JP, Waxman SG. Mutations in sodium-channel gene SCN9A cause a spectrum of human genetic pain disorders. J Clin Invest. 2007;117(12):3603-9.
59. Blesneac I, Themistocleous AC, Fratter C, Conrad LJ, Ramirez JD, Cox JJ, et al. Rare NaV1.7 variants associated with painful diabetic peripheral neuropathy. Pain. 2018;159(3):469-80.
60. Faber CG, Hoeijmakers JG, Ahn HS, Cheng X, Han C, Choi JS, et al. Gain of function Nav1.7 mutations in idiopathic small fiber neuropathy. Ann Neurol. 2012;71(1):26-39.
61. Yang Y, Wang Y, Li S, Xu Z, Li H, Ma L, et al. Mutations in SCN9A, encoding a sodium channel alpha subunit, in patients with primary erythermalgia. J Med Genet. 2004;41(3):171-4.
62. Theile JW, Jarecki BW, Piekarz AD, Cummins TR. Nav1.7 mutations associated with paroxysmal extreme pain disorder, but not erythromelalgia, enhance Navbeta4 peptide-mediated resurgent sodium currents. J Physiol. 2011;589(Pt 3):597-608.

63. Choi JS, Dib-Hajj SD, Waxman SG. Inherited erythermalgia: limb pain from an S4 charge-neutral Na channelopathy. Neurology. 2006;67(9):1563-7.
64. Cummins TR, Dib-Hajj SD, Waxman SG. Electrophysiological properties of mutant Nav1.7 sodium channels in a painful inherited neuropathy. J Neurosci. 2004;24(38):8232-6.
65. Lampert A, O'Reilly AO, Reeh P, Leffler A. Sodium channelopathies and pain. Pflügers Archiv - European Journal of Physiology. 2010;460(2):249-63.
66. Fertleman CR, Baker MD, Parker KA, Moffatt S, Elmslie FV, Abrahamsen B, et al. SCN9A mutations in paroxysmal extreme pain disorder: allelic variants underlie distinct channel defects and phenotypes. Neuron. 2006;52(5):767-74.
67. Dib-Hajj SD, Estacion M, Jarecki BW, Tyrrell L, Fischer TZ, Lawden M, et al. Paroxysmal extreme pain disorder M1627K mutation in human Nav1.7 renders DRG neurons hyperexcitable. Mol Pain. 2008;4:37.
68. McDermott LA, Weir GA, Themistocleous AC, Segerdahl AR, Blesneac I, Baskozos G, et al. Defining the Functional Role of Na(V)1.7 in Human Nociception. Neuron. 2019;101(5):905-19.e8.
69. McAllister RM, Isaacs H, Rongey R, Peer M, Au W, Soukup SW, et al. Establishment of a human medulloblastoma cell line. Int J Cancer. 1977;20(2):206-12.
70. Ngum NM, Aziz MYA, Mohammed Latif L, Wall RJ, Duce IR, Mellor IR. Non-canonical endogenous expression of voltage-gated sodium channel Na(V) 1.7 subtype by the TE671 rhabdomyosarcoma cell line. J Physiol. 2022;600(10):2499-513.
71. Burton MJ, Mellor IR, Duce IR, Davies TGE, Field LM, Williamson MS. Differential resistance of insect sodium channels with kdr mutations to deltamethrin, permethrin and DDT. Insect Biochemistry and Molecular Biology. 2011;41(9):723-32.
72. Choi JS, Soderlund DM. Structure-activity relationships for the action of 11 pyrethroid insecticides on rat Na v 1.8 sodium channels expressed in Xenopus oocytes. Toxicol Appl Pharmacol. 2006;211(3):233-44.
73. Meacham CA, Brodfuehrer PD, Watkins JA, Shafer TJ. Developmentally-regulated sodium channel subunits are differentially sensitive to α-cyano containing pyrethroids. Toxicology and Applied Pharmacology. 2008;231(3):273-81.
74. Smith TJ, Soderlund DM. Potent Actions of the Pyrethroid Insecticides Cismethrin and Cypermethrin on Rat Tetrodotoxin-Resistant Peripheral Nerve (SNS/PN3) Sodium Channels Expressed in Xenopus Oocytes. Pesticide Biochemistry and Physiology. 2001;70(1):52-61.
75. Soderlun DM, Lee SH. Point mutations in homology domain II modify the sensitivity of rat Nav1.8 sodium channels to the pyrethroid insecticide cismethrin. Neurotoxicology. 2001;22(6):755-65.
76. Tan J, Soderlund DM. Human and rat Nav1.3 voltage-gated sodium channels differ in inactivation properties and sensitivity to the pyrethroid insecticide tefluthrin. Neurotoxicology. 2009;30(1):81-9.
77. Vais H, Williamson MS, Goodson SJ, Devonshire AL, Warmke JW, Usherwood PN, et al. Activation of Drosophila sodium channels promotes modification by deltamethrin. Reductions in affinity caused by knock-down resistance mutations. J Gen Physiol. 2000;115(3):305-18.
78. Tan J, Choi JS, Soderlund DM. Coexpression with Auxiliary β Subunits Modulates the Action of Tefluthrin on Rat Na(v)1.6 and Na(v)1.3 Sodium Channels. Pestic Biochem Physiol. 2011;101(3):256-64.
79. Ginsburg KS, Narahashi T. Differential sensitivity of tetrodotoxin-sensitive and tetrodotoxin-resistant sodium channels to the insecticide allethrin in rat dorsal root ganglion neurons. Brain Research. 1993;627(2):239-48.
80. Ginsburg K, Narahashi T. Time course and temperature dependence of allethrin modulation of sodium channels in rat dorsal root ganglion cells. Brain Res. 1999;847(1):38-49.

81. Erin NW, April PN, William DA. Pyrethroids and Their Effects on Ion Channels. In: Soundararajan RP, editor. Pesticides. Rijeka: IntechOpen; 2012. p. Ch. 3.
82. Soderlund DM. Molecular mechanisms of pyrethroid insecticide neurotoxicity: recent advances. Arch Toxicol. 2012;86(2):165-81.
83. Han C, Dib-Hajj SD, Lin Z, Li Y, Eastman EM, Tyrrell L, et al. Early- and late-onset inherited erythromelalgia: genotype–phenotype correlation. Brain. 2009;132(7):1711-22.
84. Soderlund DM. Molecular mechanisms of pyrethroid insecticide neurotoxicity: recent advances. Archives of Toxicology. 2012;86(2):165-81.
85. Silver KS, Du Y, Nomura Y, Oliveira EE, Salgado VL, Zhorov BS, et al. Voltage-Gated Sodium Channels as Insecticide Targets. Adv In Insect Phys. 2014;46:389-433.
86. Flannigan SA, Tucker SB, Key MM, Ross CE, Fairchild EJ, 2nd, Grimes BA, et al. Synthetic pyrethroid insecticides: a dermatological evaluation. Br J Ind Med. 1985;42(6):363-72.
87. Cagen SZ, Malley LA, Parker CM, Gardiner TH, Van Gelder GA, Jud VA. Pyrethroid-mediated skin sensory stimulation characterized by a new behavioral paradigm. Toxicology and Applied Pharmacology. 1984;76(2):270-9.
88. Tan J, Soderlund DM. Actions of Tefluthrin on Rat Na(v)1.7 Voltage-Gated Sodium Channels Expressed in Xenopus Oocytes. Pestic Biochem Physiol. 2011;101(1):21-6.
89. Wolansky MJ, Gennings C, Crofton KM. Relative potencies for acute effects of pyrethroids on motor function in rats. Toxicol Sci. 2006;89(1):271-7.
90. Thull S, Neacsu C, O'Reilly AO, Bothe S, Hausmann R, Huth T, et al. Mechanism underlying hooked resurgent-like tail currents induced by an insecticide in human cardiac Nav1.5. Toxicology and Applied Pharmacology. 2020;397:115010.
91. Soderlund DM, Tan J, He B. Functional reconstitution of rat Nav1.6 sodium channels in vitro for studies of pyrethroid action. NeuroToxicology. 2017;60:142-9.
92. Usherwood PN, Davies TG, Mellor IR, O'Reilly AO, Peng F, Vais H, et al. Mutations in DIIS5 and the DIIS4-S5 linker of Drosophila melanogaster sodium channel define binding domains for pyrethroids and DDT. FEBS Lett. 2007;581(28):5485-92.
93. Peng F, Mellor IR, Williamson MS, Davies TG, Field LM, Usherwood PN. Single channel study of deltamethrin interactions with wild-type and mutated rat Na(V)1.2 sodium channels expressed in Xenopus oocytes. Neurotoxicology. 2009;30(3):358-67.
94. Trainer VL, McPhee JC, Boutelet-Bochan H, Baker C, Scheuer T, Babin D, et al. High affinity binding of pyrethroids to the alpha subunit of brain sodium channels. Mol Pharmacol. 1997;51(4):651-7.
95. Dong K. Insect sodium channels and insecticide resistance. Invert Neurosci. 2007;7(1):17-30.
96. Vais H, Atkinson S, Pluteanu F, Goodson SJ, Devonshire AL, Williamson MS, et al. Mutations of the para sodium channel of Drosophila melanogaster identify putative binding sites for pyrethroids. Mol Pharmacol. 2003;64(4):914-22.
97. O'Reilly AO, Khambay BP, Williamson MS, Field LM, Wallace BA, Davies TG. Modelling insecticide-binding sites in the voltage-gated sodium channel. Biochem J. 2006;396(2):255-63.